Supplementary Information for：

Mapping immune imprinting zones enables predictive vaccination optimization

Supplementary Note 1: Mathematical modeling of humoral immunity with DynaVac

1.1 Overview of the humoral immune response and model structure

Humoral immunity to viral infection or vaccination proceeds through well-defined stages, including antigen presentation, B cell activation, affinity maturation, and antibody secretion. Upon initial exposure, naive B cells generated through V(D)J recombination in the bone marrow circulate to secondary lymphoid tissues, where they encounter antigen for the first time[1-3]. These cells typically express low-affinity B cell receptors (BCRs), but if the BCR binds antigen with sufficient affinity—such as viral surface proteins—naive B cells are activated and recruited into germinal center reactions[4].

Within germinal centers, activated B cells undergo clonal expansion and acquire somatic hypermutations mediated by activation-induced cytidine deaminase (AID)[5]. The resulting BCR variants exhibit a spectrum of affinities. High-affinity clones are preferentially selected through interactions with follicular dendritic cells and helper T cells, which provide survival and differentiation signals[6]. B cells failing to receive these cues are eliminated by apoptosis[7]. This iterative Darwinian process—termed affinity maturation—progressively enriches for clones with improved antigen binding[8].

Affinity-matured B cells adopt one of two fates: differentiation into plasma cells that secrete antigen-specific antibodies, or entry into the memory B cell pool[9]. Memory B cells persist in a quiescent state, maintaining high-affinity BCRs and enabling rapid recall upon subsequent antigen exposure. When re-exposed to antigenically similar variants, memory B cells dominate the secondary response, often outcompeting naive B cells—a phenomenon known as immune imprinting[10,11]. Depending on the antigenic relationship between priming and boosting antigens, imprinting can either enhance protection or suppress variant-specific responses.

To quantitatively capture these dynamics, we developed DynaVac, a mechanistic model based on ordinary differential equations (ODEs) that simulates the evolution of key components of humoral immunity following sequential exposures to antigenically distinct viral variants. By using mean-field approximations, DynaVac represents polyclonal B cell and antibody populations as effective monoclonal entities, balancing biological realism with computational tractability. The model is structured in two phases: (1) the primary phase, capturing immune dynamics following the first antigen exposure, and (2) the booster phase, simulating responses to subsequent homologous or heterologous antigens. These components are detailed in the sections that follow.

1.2 Primary phase (initial antigen exposure)

This phase models the humoral immune response following the first exposure to an antigen (e.g., prototype SARS-CoV-2). It tracks five key immune variables:
R: mRNA level
Ag: Antigen level
N: Gross affinity of the naive B cell population
M: Memory B cell level
Ab: Antibody level
The temporal behavior of these variables is governed by the following ordinary differential equations:

$$\frac{dR}{dt} = -\gamma_R R \tag{1}$$

$$\frac{dAg}{dt} = kR - \gamma_c K_a Ag Ab - \gamma_{Ag} Ag \tag{2}$$

$$\frac{dN}{dt} = a(t)s_{ini} + a_N(t)s_N f(Ag,K)N(1-N) - d_N N \quad (3)$$

$$\frac{dM}{dt} = k_{N2M}N(1-M) - d_M M \quad (4)$$

$$\frac{dAb}{dt} = a_N(t)p_N N - \gamma_{Ab}Ab \quad (5)$$

Equation 1 models the degradation of mRNA following vaccine administration, with γ_R representing the decay rate.

Equation 2 describes antigen kinetics. Antigen (e.g. SARS-CoV-2 Spike protein) is produced from mRNA at rate k and degraded through two processes: intrinsic decay (γ_{Ag}) and immune-mediated clearance via antigen-antibody binding. Under the quasi-steady-state assumption, the antigen-antibody complex $[Ag{:}\,Ab]$ is modeled as $K_a[Ag][Ab]$, where K_a is the binding affinity constant. The degradation rate of this complex is set as γ_c. This formulation captures the dynamic interplay between antibody availability and antigen clearance, reflecting the essential feedback between humoral responses and antigen persistence.

Equation 3 models naive B cell dynamics using a mean-field approximation.

The variable $N \in [0,1]$ (Gross affinity of the naive B cell population) represents the ***normalized product of two dimensions***: (1) the average antigen affinity of naive B cell receptors (BCRs) and (2) the population size of naive B cells. This combined metric captures that germinal center (GC) reactions *simultaneously* enhance affinity through somatic hypermutation and expand high-affinity clones (Victora and Nussenzweig, 2022). When $N = 1$, it indicates both maximal average affinity and population size within GC capacity constraints.

During the early stage of a humoral immune response, progenitor naive B cells that have undergone VDJ recombination enter lymph nodes to seed germinal centers. For simplicity, the parameter s_{ini} denotes the constant innate maturation rate of the gross affinity N during this seeding process. The time window of the above process is represented by $a(t)$, a rectangular function:

$$a(t) = \begin{cases} 1, & t_0 \le t < t_0 + t_{ini} \\ 0, & t_0 + t_{ini} \le t \end{cases}$$

where t_0 denotes the vaccination timepoint, t_{ini} is the time interval before germinal center reactions commence, during which progenitor naive B cells seed the lymph nodes.

Germinal center reactions subsequently occur, wherein antigen-specific naive B cells proliferate under somatic hypermutation and T cell selection, increasing the gross affinity N.

The affinity maturation process is driven by successful binding of naive B cell receptors (BCRs) to antigens presented on follicular dendritic cells (FDCs). This binding efficiency is modeled as the product of three interdependent factors: ***antigen accessibility***, ***the population size of naive B cells***, and their ***average antigen affinity***.

Antigen accessibility is captured by the function $f(Ag,K) = \frac{Ag}{Ag+K}$, where Ag represents the antigen concentration and K is a composite parameter reflecting the FDC's maximum antigen-presenting capacity. This formulation mirrors saturation kinetics, where antigen presentation level increases linearly at low antigen levels ($\mathrm{Ag} \ll \mathrm{K}$) and plateaus as FDC surfaces become saturated ($Ag \gg K$). The ***naive B cell population size*** and their ***average antigen affinity*** are combined into a single variable by the integrated metric N, explicitly coupling clonal expansion (population size) and affinity maturation (improved BCR-antigen binding) during germinal center reactions.

To enforce biological realism, the term $(1-N)$ imposes a saturation constraint, ensuring N asymptotically approaches 1. This constraint arises from two inseparable limits: the finite physical space within germinal centers that restricts clonal expansion, and the biophysical ceiling of BCR-antigen interactions.

The resultant maturation rate $s_N \frac{Ag}{Ag+K} N(1-N)$ dynamically integrates antigen availability $\frac{Ag}{Ag+K}$, population gross antigen affinity N, and system-wide saturation $1-N$, faithfully recapitulating the competitive and self-limiting nature of affinity maturation observed in vivo. Maximal maturation s_N occurs under antigen saturation ($f(Ag,K) \to 1$) and minimal population gross affinity ($N \to 0, (1-N) \to 1$), where both affinity-driven selection and affinity maturation potential are optimized.

The window $a_N(t)$ delineates the naive immune response timespan:

$$a_N(t) = \begin{cases} 1, (t_0 + t_{ini} \le t < t_0 + t_{ini} + t_{min}) \; or \; [(t_0 + t_{ini} + t_{min} \le t < t_0 + t_{ini} + t_{max}) \; and \; (Ag > 0)] \\ 0, \; otherwise \end{cases} \quad (6)$$

where t_{min} and t_{max} are the minimum and maximum immune response durations. Reactions persist for at least t_{min} and between t_{min} and t_{max} depending on remaining antigens ($Ag > 0$). Beyond t_{max}, reactions cease.
Additionally, naive B cells decay at rate d_N.

Equation 4 models memory B cell formation as a function of the gross affinity of naive B cell N, as a higher N directly represents a larger affinity-matured naïve B cell pool. The formation rate scales with N and is constrained by a carrying capacity term $(1 - M)$ and a decay rate d_M.

Equation 5 tracks antibody secretion. Analogous to memory B cell differentiation, antibodies are produced in proportion to the gross affinity of naive B cell (N), modulated by production rate p_N, and decay at rate γ_{Ab}. The parameter p_N aggregates the differentiation of mature naïve B cells into antibody-secreting plasma cells and their subsequent antibody secretion, implicitly modeling plasma cells without explicitly tracking their transient dynamics or lifespan.

These equations collectively describe how antigen exposure drives naive B cell recruitment, affinity maturation, memory formation, and antibody production in the primary immune response.

1.3 Booster Phase (Subsequent Antigen Exposures)

The booster phase accounts for immune responses following additional exposures, particularly to antigenically distinct variants. Recall responses are explicitly modeled through both naive and memory B cell dynamics.

1.3.1 Modeling homologous boost

In secondary immune responses to homologous boosters, antibody production arises from both naive and memory compartments. Although early studies proposed that memory B cells could re-enter germinal centers for further maturation, recent findings suggest that secondary germinal centers are predominantly (>90%) populated by naive B cells, with minimal memory B cell re-entry [12,1314]. Thus, our model excludes memory B cell re-entry into germinal centers. Instead, memory B cells are reactivated primarily outside germinal centers, within structures like subcapsular proliferative foci (SPFs), where they proliferate in an affinity-dependent manner and differentiate into antibody-secreting plasma cells[15,16].

We define two memory B cell populations: inactive memory cells (M^{off}) generated during the primary phase, and activated memory cells (M^{on}), formed upon secondary exposure. For simplicity, we assume M^{off} rapidly converts to M^{on} immediately following boost.

Activated memory cells proliferate in an affinity-dependent fashion, modeled analogously to naive B cells as: $s_M \frac{Ag}{Ag+K} M^{on}\left(1 - M^{on} - M^{off}\right)$, where s_M denotes the maximal memory proliferation rate. These cells also contribute to antibody production with aggregate rate p_M. As explained earlier in the primary antibody dynamics (**Equation 5**), this rate implicitly incorporates both the differentiation of memory cells into plasma cells and the antibody secretion by these plasma cells.
Memory response are confined within a defined temporal window:

$$a_M(t) = \begin{cases} 1, (t_0 \le t < t_0 + t_{ini} + t_{min}) \wedge [(t_0 + t_{ini} + t_{min} \le t < t_0 + t_{ini} + t_{max}) \vee (Ag > 0)] \\ 0, \; otherwise \end{cases}$$

Considering the rapid nature of memory B cell activation upon secondary vaccination, this process is modeled as occurring immediately at the boost timepoint t_0, maintaining identical duration parameters as established for the naive immune response $a_N(t)$.
By incorporating the dynamics of M_{on} into the primary response framework, we can simulate homologous antigen boosting in an integrated framework:

$$\frac{dR}{dt} = -\gamma_R R \tag{7}$$

$$\frac{dAg}{dt} = kR - \gamma_c K_a Ag Ab - \gamma_{Ag} Ag \tag{8}$$

$$\frac{dN}{dt} = a_{in}(t)s_{in} + a_N(t)s_N \frac{Ag}{Ag+K} N(1-N) - d_N N \tag{9}$$

$$\frac{dM_{off}}{dt} = k_{N2M} N\left(1 - M_{on} - M_{off}\right) - d_M M_{off} \tag{10}$$

$$\frac{dM_{on}}{dt} = a_M(t)s_M \frac{Ag}{Ag+K} M_{on}\left(1 - M_{on} - M_{off}\right) - d_M M_{on} \tag{11}$$

$$\frac{dAb}{dt} = a_N(t)p_N N + a_M(t)p_M M_{on} - \gamma_{Ab} Ab \tag{12}$$

1.3.2 Modeling heterologous boost

To address responses to heterologous exposures—common with SARS-CoV-2 variants—we extended DynaVac to simulate variant-specific antigen dynamics. The model tracks *n* distinct variants, denoted by subscript *i*, including antigen (Ag_i), naive B cells (N_i), inactive and activated memory B cells (M_i^{off}, M_i^{on}), and antibodies (Ab_i).

Based on **Equations 7-12**, the extended ODE system is:

$$\frac{dR_i}{dt} = -\gamma_R R_i \tag{13}$$

$$\frac{dAg_i}{dt} = kR_i - \gamma_c \sum_j^n Ka_j c_{i,j}\, Ag_i Ab_j - \gamma_{Ag} Ag_i \tag{14}$$

$$\frac{dN_i}{dt} = a_N(t)s_N \frac{Ag_i}{Ag_i+K} N_i(1-N_i) - d_N N_i \tag{15}$$

$$\frac{dM_i^{off}}{dt} = k_{N2M} N_i \left[1 - \sum_j^n \left(M_j^{off} + M_j^{on}\right)\right] - d_M M_i^{off} \tag{16}$$

$$\frac{dM_i^{on}}{dt} = a_M(t)s_M \left(\sum_k^n \frac{Ag_k}{Ag_k+K} \frac{Ka_k c_{i,k} M_i^{on}}{\sum_j^n Ka_k c_{j,k} M_j^{on} + m_0}\right) M_i^{on} \left[1 - \sum_j^n \left(M_j^{off} + M_j^{on}\right)\right] - d_M M_i^{on} \tag{17}$$

$$\frac{dAb_i}{dt} = a_N(t)p_N N_i + a_M(t) \frac{p_M c_{i,k}}{c_{i,k}+c_0} M_i^{on} - \gamma_{Ab} Ab_i \tag{18}$$

The following are additional key considerations in the above equations:

1) Cross-neutralization: Each antigen variant Ag_i can be neutralized by different variant-specific antibodies , represented by $\gamma_c \sum_j^n Ka_j c_{i,j}\, Ag_i Ab_j$ in **Equation 14,** where $c_{i,j}$ represents the cross-neutralization coefficient. To quantify this, we define the cross-neutralization coefficient as:

$$c_{i,j} = Ka_{i,j}/Ka_j \tag{19}$$

where $Ka_{i,j}$ is the affinity constant of variant j-specific antibodies toward antigen variant i, and Ka_j is the self-affinity constant of variant j-specific antibodies. By definition, $c_{i,i} = 1$, indicating strongest affinity for matched antigens, and $c_{i,j} \in (0,1)$ for $i \neq j$. Thus, a higher $c_{i,j}$ implies stronger cross-neutralization.

2) Memory B cell competition: Upon exposure to antigen *k*, memory B cells specific to various antigens compete for proliferation signals based on their affinity and population size. A population's competitive advantage depends on the antigen-binding potential ($Ka_k c_{i,k} M_i^{on}$). To reflect this competition, the antigen-dependent proliferation rate for each memory cell population is normalized by the total antigen-binding potential across all memory populations $\sum_j^n Ka_k c_{j,k} M_j^{on}$. Furthermore, the proliferation of a memory cell population M_i^{on} in response to a cross-reactive antigen depends on whether its antigen-binding potential surpasses a threshold m_0. Specifically, proliferation is maximized if $Ka_k c_{i,k} M_i^{on}$ greatly exceeds m_0, significantly reduced as it approaches m_0, and minimal if it falls far below m_0.

3) Antibody attenuation: Memory B cells (e.g., M_i^{on}) activated by an antigen variant (e.g., Ag_k) different from their original specificity differentiate into plasma cells and secrete antibody (Ab_i) less efficiently , modeled by the term $\frac{c_{i,k}}{c_{i,k}+c_0}$, with c_0 as the cross-reactivity threshold below which secretion is substantially reduced.

This extended framework enables mechanistic simulation of sequential heterologous exposures involving multiple antigen variants and captures phenomena such as cross-neutralization, immune imprinting, and competitive memory dynamics.

1.4 Key simplification of the model

To balance biological realism with computational tractability, DynaVac adopts a mean-field approximation, representing the naive B cells, memory B cells, and antibody responses to each antigen variant with single aggregated variables. In reality, these populations are polyclonal—comprising diverse B cell clones with distinct BCRs that arise through stochastic processes of V(D)J recombination, somatic hypermutation, and selection. This clonal diversity leads to antibodies with a range of affinities even when targeting the same antigen[6]. By modeling these processes deterministically, the framework captures the overall behavior of the immune response without explicitly tracking individual clones. The affinity constant Ka_i reflects the average binding affinity of antibody i to antigen i across the polyclonal repertoire. The variable N represents the gross affinity maturity of the entire naive B cell population, encompassing both size and average antigen affinity.

This simplification significantly enhances computational efficiency and predictive capacity, enabling rapid simulation of diverse vaccination scenarios. Similar mean-field approaches have been successfully employed in prior immunological modeling studies and can effectively substitute for fully stochastic models in most settings [21].

1.5 Prior estimation of parameters interval

All model parameters governing the full system of DynaVac (**Equations 13–18**) are listed in Supplementary Table 1. To facilitate robust and biologically grounded parameter inference, we established prior intervals for each parameter based on a combination of published experimental data and previous modeling efforts (Supplementary Table 1). For novel parameters introduced in this study—those lacking direct empirical estimates—we defined conservative bounds informed by biological plausibility, ensuring both interpretability and computational stability during model fitting.

1.6 Model reduction

We next simplified the model to reduce complexity without compromising accuracy.

1.6.1 Simplification of the mRNA translation process

The translation of mRNA into antigen, when considered in isolation, can be described by simple linear ODEs:

$$\frac{dR}{dt} = -\gamma_R R$$
$$\frac{dAg}{dt} = kR$$

Given an injected mRNA vaccine dose of m ug, the initial conditions become:

$$R(0) = mR_0$$
$$Ag(0) = 0$$

Solving these equations yields:

$$R(t) = mR_0 e^{-\gamma_R t}$$
$$Ag(t) = \frac{kmR_0}{\gamma_R}(1 - e^{-\gamma_R t})$$

As $t \to \infty$, the total antigen translated from m ug of mRNA vaccine is $\frac{kmR_0}{\gamma_R}$. Define t_{99} as the time required for translating 99% of this total antigen, which satisfies:

$$1 - e^{-\gamma_R t_{99}} = 0.99 \Rightarrow t_{99} = \frac{ln100}{\gamma_R}$$

According to prior estimates for γ_R (Supplementary Table 1), t_{99} is less than one day, implying rapid antigen translation due to fast mRNA degradation. Considering that the initiation of antibody production ($t_{ini} \in [0.5,2]$, Supplementary Table 1) occurs around or after this period, we conclude the explicit mRNA translation and degradation steps can be omitted. Instead, an equivalent initial antigen concentration $Ag(t_0) = mP_r$ is introduced, where $P_r = \frac{kR_0}{\gamma_R}$ represents the amount of

antigen generated per μg of mRNA. This simplification reduces model dimensionality and consolidates three parameters into one, with a prior interval approximately estimated as $P_r \approx [5,30] * 10^{11}$ M/ug.

1.6.2 Simplification of antigen-antibody neutralization parameters

In the original model, antigen-antibody neutralization terms appear as a product of two parameters: the antigen-antibody complex degradation rate γ_c and the affinity constant K_{a_i} (see **Equation. 14**). For simplicity, we combine these parameters into a single variant-specific neutralization rate $\gamma_{neu_i} = \gamma_c K_{a_i}$, representing the rate of neutralization of antigen Ag_i by its specific antibody Ab_i.

1.6.3 Simplification of parameter units

Parameters P_s, P_v, and the newly defined P_r have units of M/ug, with magnitudes around 10^{-12}. To simplify parameter magnitudes and facilitate estimation, we rescale the units of these parameters to 10^{-12} M/ug. Correspondingly, for unit consistency, parameter K is rescaled from M to 10^{-12} M and the affinity constant Ka from M^{-1} to 10^{12} M^{-1}.

After implementing these simplifications, the original ODEs (**Equations 13-18**) reduces to:

$$\frac{dAg_i}{dt} = -\sum_j^n \gamma_{neu_i} c_{i,j}\, Ag_i Ab_j - \gamma_{Ag} Ag_i \quad (20)$$

$$\frac{dN_i}{dt} = a_N(t) s_N f(Ag_i, K) N_i (1 - N_i) - d_N N_i \quad (21)$$

$$\frac{dM_i^{off}}{dt} = k_{N2M} N_i \left[1 - \sum_j^n \left(M_j^{off} + M_j^{on}\right)\right] - d_M M_i^{off} \quad (22)$$

$$\frac{dM_i^{on}}{dt} = a_M(t) s_M \left(\sum_k^n \frac{Ag_k}{Ag_k + K} \frac{\gamma_{neu_k} c_{i,k} M_i^{on}}{\sum_j^n \gamma_{neu_k} c_{j,k} M_j^{on} + m_0}\right) M_{on_i} \left[1 - \sum_j^n \left(M_j^{off} + M_j^{on}\right)\right] - d_M M_i^{on} \quad (23)$$

$$\frac{dAb_i}{dt} = a_N(t) p_N N_i + a_M(t) \frac{p_M M_i^{on} c_{i,k}}{c_{i,k} + c_0} - \gamma_{neu_i} \sum_j^n c_{j,i}\, Ag_j Ab_i - \gamma_{Ab} Ab_i \quad (24)$$

The parameters and their updated prior intervals for this reduced model are provided in Supplementary Table 2.

Supplementary Note 2: DynaVac-based vaccination regimens simulation and parameter estimation using experimental data

2.1 Estimating variant-specific self-neutralization rate and the cross-neutralization matrix using homologous vaccination regimens

Among the 29 vaccination regimens designed (Fig. 2a, main text), seven involved two-doses homologous vaccinations of monovalent vaccine—specifically CoronaVac or mRNA-based formulations targeting the Alpha/Beta, Delta, BA.1, BA.2/4/5, XBB.1.5, or JN.1 variants—in the absence of prior immune imprinting. These regimens elicit "pure" antibody responses induced by a single antigen, enabling direct estimation of the variant-specific self-neutralization rates, denoted as $\mathbf{\Gamma_{neu}}$, and the cross-neutralization matrix $\mathbf{C}$.

Raw pseudovirus neutralization titers for these regimens are summarized in Supplementary Table 3, each reflecting the geometric mean titer (GMT) across eight replicate experiments. To construct a 7×7 cross-neutralization matrix $\mathbf{C}$, neutralization titers against the hypothetical Alpha/Beta and BA.2/5 fusion antigens are required. F These were approximated by taking the geometric mean of the GMTs for the corresponding individual components (Supplementary Table 4).

Let $\mathbf{T} = \left(T_{i,j}\right)_{7\times7}$ represent the resulting titer matrix, in which $T_{i,j}$ denotes the neutralization titer of antigen j -induced antibody against antigen i . Diagonal elements ($T_{i,i}$) represent self-neutralization titers and are provided in Supplementary Table 5. Under standardized vaccine type and dosage (e.g., 30 μg mRNA vaccines for Alpha/Beta, Delta, BA.1, BA.2/4/5, XBB.1.5), these self-neutralization titers scale with the relative magnitudes of variant-specific self-neutralization rates $\mathbf{\Gamma_{neu}} = \left(\gamma_{neu_1}, \gamma_{neu_2}, \ldots, \gamma_{neu_n}\right)$.

To enable relative comparison across variants, we introduce the Delta-variant-specific self-neutralization rate (γ_{neu}^{Delta}) as a reference standard. We define the vector of relative self-neutralization ratios (f_i^{Delta}) as (Supplementary Table 5):

$$f_i^{Delta} = \frac{T_{i,i}}{T_{Delta,Delta}} = \frac{\gamma_{neu,i}}{\gamma_{neu}^{Delta}}$$

The relative self-neutralization ratio for CoronaVac (prototype-targeting inactivated vaccine administered at 5 μg), denoted $f_{CoronaVac}^{\mathrm{Delta}}$, cannot be directly compared using this framework and is thus estimated independently. Both γ_{neu}^{Delta} and $f_{CoronaVac}^{\mathrm{Delta}}$ are treated as free parameters and are jointly inferred through the model optimization procedure described in Supplementary Note 2.3.

Having defined f_i^{Delta} and established γ_{neu}^{Delta} as a scaling anchor, the absolute neutralization rate of each variant can be reconstructed as:

$$\gamma_{neu,i} = f_i^{Delta} \times \gamma_{neu}^{Delta}$$

The cross-neutralization matrix ($\mathbf{C}$) is calculated by normalizing off-diagonal titers relative to their corresponding self-titers:

$$c_{i,j} = \frac{T_{i,j}}{T_{j,j}}$$

The resulting cross-neutralization matrix is provided in Supplementary Table 6.

2.2 Vaccination regimens simulation using DynaVac

2.2.1 Monovalent vaccination strategy simulation

Having established the variant-specific self-neutralization rates $\mathbf{\Gamma_{neu}} = \left(\gamma_{neu_1}, \gamma_{neu_2}, \ldots, \gamma_{neu_n}\right)$ and the cross-neutralization matrix $\mathbf{C} = \left(c_{i,j}\right)_{n\times n}$, these parameters are incorporated as essential inputs to the DynaVac simulation framework.

To simulate immune responses following a vaccination regimen involving n variants and m sequential immunizations, we represent the regimen using four vectors:

- $\boldsymbol{T} = (t_{01}, t_{02}, ..., t_{0m})$: time points (in days) of each vaccination, with $0 \leq t_{01} < t_{02} < ... < t_{0m}$.
- $\boldsymbol{V} = (v_1, v_2, ..., v_m)$: variant index of each vaccine dose, where $v_k \in \{1,2,...,n\}$.
- $\boldsymbol{D} = (d_1, d_2, ..., d_m)$: antigen dose (μg) for each vaccination;
- $\boldsymbol{P} = (p_1, p_2, ..., p_m)$: vaccine type (1: protein, 2: mRNA, 3: inactivated).

Simulations proceed by numerically solving the initial value problem defined by the system of ODEs (Equations 20–24) for each vaccination interval $[t_{0k}, t_{0k+1})$ sequentially.

Denote the solution for the k-th vaccination period $[t_{0k}, t_{0k+1})$ as:

$$\left[\boldsymbol{Ag_k}(t), \boldsymbol{N_k}(t), \boldsymbol{M_{off_k}}(t), \boldsymbol{M_{on_k}}(t), \boldsymbol{Ab_k}(t)\right]$$

The initial conditions for the first vaccination ($k = 1$), the initial conditions are:

$$Ag_{1,i}(t_{01}) = \begin{cases} d_1 P_s, & v_1 = i \text{ and } p_1 = 1 \\ d_1 P_r, & v_1 = i \text{ and } p_1 = 2 \\ d_1 P_v, & v_1 = i \text{ and } p_1 = 3 \\ 0, & v_1 \neq i \end{cases}$$

$$\boldsymbol{N_1}(t_{01}) = \boldsymbol{M_{off_1}}(t_{01}) = \boldsymbol{M_{on_1}}(t_{01}) = \boldsymbol{Ab_1}(t_{01}) = \boldsymbol{0}$$

For subsequent vaccinations ($1 < k \leq m$), the initial conditions are:

Antigen initial condition:

$$Ag_{k,i}(t_{0k}) = \begin{cases} Ag_{k-1,i}(t_{0k}) + d_k P_s, & v_k = i \text{ and } p_k = 1 \\ Ag_{k-1,i}(t_{0k}) + d_k P_r, & v_k = i \text{ and } p_k = 2 \\ Ag_{k-1,i}(t_{0k}) + d_k P_v, & v_k = i \text{ and } p_k = 3 \\ Ag_{k-1,i}(t_{0k}), & v_k \neq i \end{cases}$$

Memory B cells and antibodies:

$$\boldsymbol{M_{off_k}}(t_{0k}) = \boldsymbol{0}, \boldsymbol{M_{on_k}}(t_{0k}) = \boldsymbol{M_{on_{k-1}}}(t_{0k}) + \boldsymbol{M_{off_{k-1}}}(t_{0k})$$

$$\boldsymbol{N_k}(t_{0k}) = \boldsymbol{N_{k-1}}(t_{0k}), \boldsymbol{Ab_k}(t_{0k}) = \boldsymbol{Ab_{k-1}}(t_{0k})$$

(Upon each new vaccination, all inactive memory B cells ($\boldsymbol{M_{off}}$) transition immediately to the activated memory pool ($\boldsymbol{M_{on}}$) at the time t_{0k}.)

Concatenating solutions across all intervals yields the complete simulation trajectory:

$$\left[\boldsymbol{Ag}(t), \boldsymbol{N}(t), \boldsymbol{M_{off}}(t), \boldsymbol{M_{on}}(t), \boldsymbol{Ab}(t)\right], t \in [t_{01}, t_{end}]$$

where $t_{end} > t_{0m}$ is the end of the simulation.

2.2.2 Multivalent vaccine vaccination strategy simulation

For vaccination strategies involving multivalent vaccines, the vector $\boldsymbol{V}$ is generalized to a $q \times m$ matrix, representing up to q antigenic components per vaccine:

$$\boldsymbol{V} = \left(v_{j,k}\right)_{q \times m}, v_{j,k} \in \{0,1,...,n\}$$

where $v_{j,k}$ represents the variant of the j-th antigenic component in the vaccine used in the k-th vaccination. If the valency of the vaccine used in the k-th vaccination, denoted as q_k, is lower than the highest vaccine valency q in the strategy, the missing antigen components are filled with 0. Specifically, for the k-th column of matrix $\boldsymbol{V}$, if $q_k < j \leq q$, then $v_{j,k} = 0$.

Initial antigen conditions are adjusted accordingly:

For the first vaccination ($k = 1$):

$$Ag_{1,i}(t_{01}) = \begin{cases} d_1 P_s / q_1, & i \in \boldsymbol{v_{\cdot 1}} \text{ and } p_1 = 1 \\ d_1 P_r / q_1, & i \in \boldsymbol{v_{\cdot 1}} \text{ and } p_1 = 2 \\ d_1 P_v / q_1, & i \in \boldsymbol{v_{\cdot 1}} \text{ and } p_1 = 3 \\ 0, & i \notin \boldsymbol{v_{\cdot 1}} \end{cases}$$

For subsequent vaccinations ($k > 1$):

$$Ag_{k,i}(t_{0k}) = \begin{cases} Ag_{k-1,i}(t_{0k}) + d_k P_s / q_k, & i \in \boldsymbol{v_{\cdot k}} \text{ and } p_k = 1 \\ Ag_{k-1,i}(t_{0k}) + d_k P_r / q_k, & i \in \boldsymbol{v_{\cdot k}} \text{ and } p_k = 2 \\ Ag_{k-1,i}(t_{0k}) + d_k P_v / q_k, & i \in \boldsymbol{v_{\cdot k}} \text{ and } p_k = 3 \\ Ag_{k-1,i}(t_{0k}), & i \notin \boldsymbol{v_{\cdot k}} \end{cases}$$

Here, q_k represents the valency of the vaccine used in the k-th vaccination, and $\boldsymbol{v_{\cdot k}}$ denotes the k-th column of matrix $\boldsymbol{V}$.

Initial conditions for memory B cells and antibodies follow the same rules as monovalent vaccination. A detailed pseudo-code for implementing arbitrary vaccination regimens using DynaVac is provided as follows:

Algorithm for Simulating Vaccination Strategy using DynaVac

Input: Vaccination times T, variant matrix V, doses D, vaccine types P, variant-specific neutralization rates Γ_neu, cross-neutralization matrix C, simulation end time t_end.

Output: Dynamics of antigen levels Ag, naive B cell levels N, inactivated memory B cell levels M_off, activated memory B cell levels M_on, antibody levels Ab.

```
n = length(Γ_neu); // Number of variants
m = length(T);     // Number of vaccinations
[Ag, N, M_off, M_on, Ab] = InitializeStates(n);
for k = 1 to m do
    if (k == 1) then
        Ag = SetAntigenLevels(V[:, 1], D[1], P[1], Ag, T[1]);
    else
        Ag = UpdateAntigenLevels(V[:, k], D[k], P[k], Ag, T[k]);
        M_off[:, T[k]] = 0;
        M_on[:, T[k]] = M_on[:, T[k]] + M_off[:, T[k]];
        N[:, T[k]] = N[:, T[k-1]];
        Ab[:, T[k]] = Ab[:, T[k-1]];
    end if
    [Ag, N, M_off, M_on, Ab] = SolveODEs(Ag, N, M_off, M_on, Ab, Γ_neu, C, T[k], T[k+1]);
end for
return [Ag, N, M_off, M_on, Ab];

function InitializeStates(n)
Ag = zeros(n,1);
N = zeros(n,1);
M_off = zeros(n,1);
M_on = zeros(n,1);
Ab = zeros(n,1);
return [Ag, N, M_off, M_on, Ab];
function SetAntigenLevels(v, d, p, Ag, t)
// Set initial antigen levels according to vaccine type and variant
function UpdateAntigenLevels(v, d, p, Ag, t)
// Update antigen levels by adding new dose to existing levels
function SolveODEs(Ag, N, M_off, M_on, Ab, Γ_neu, C, t_start, t_end)
// Numerically solve the ODEs for the given time interval
```

2.3 Estimation of remaining parameters using 29 vaccination regimens in this study

Let $\overline{\mathbf{T}} = \left(\overline{T}_{i,j}\right)_{11\times7}$ denote the matrix of GMTs for 7 homologous vaccination regimens against the 11 pseudoviruses (Supplementary Table 7). Each element $\overline{T}_{i,j}$ represents the neutralization titer of variant j-specific antibody against pseudovirus i.

The antibody-pseudovirus cross-neutralization coefficients $\overline{c}_{i,j}$ are defined as:

$$\overline{c}_{i,j} = \frac{\overline{T}_{i,j}}{T_{j,j}}$$

where $T_{j,j}$ is the self-neutralization titer of variant j-specific antibody (Supplementary Table 5). Using this definition, we obtain the antibody-pseudovirus cross-neutralization matrix $\overline{\mathbf{C}} = \left(\overline{c}_{i,j}\right)_{11\times7}$ (Supplementary Table 8).

We define the parameter vector $\boldsymbol{\theta}$, which contains the 28 unknown parameters listed in Supplementary Table 2.

For each vaccination regimen indexed by l, immune response trajectories are simulated using DynaVac based on its encoded vectors $\boldsymbol{T_l, V_l, D_l, P_l}$ as described in Supplementary Notes 2.1. Given a parameter set $\boldsymbol{\theta}$, the simulated variant-specific antibody concentrations at any time t are denoted as:

$$\boldsymbol{Ab_l}(t, \boldsymbol{T_l, V_l, D_l, P_l}, \boldsymbol{\theta})$$

The simulated antibody concentrations at the measurement time point t_{lm} (14 days after the last dose) are denoted as:

$$\boldsymbol{Ab_{lm}}(\boldsymbol{\theta}) = \boldsymbol{Ab_l}(t_{lm}; \boldsymbol{T_l, V_l, D_l, P_l}, \boldsymbol{\theta})$$

Based on equilibrium assumptions, the neutralization titer of a mixed antibody population against pseudovirus k (NT_k) is proportional to the weighted sum of antibody levels multiplied by their neutralization rates and cross-neutralization coefficients (See the Appendix for a detailed proof):

$$NT_k \propto \sum_{j=1}^{n} \gamma_{neu_j} \overline{c}_{k,j} Ab_j = \overline{\boldsymbol{c}}_{\boldsymbol{k}:} \cdot (\boldsymbol{\Gamma_{neu}} \circ \boldsymbol{Ab}) \quad (25)$$

Here, $\overline{\boldsymbol{c}}_{\boldsymbol{k}:}$ represents the k-th row of the antibody-pseudovirus cross-neutralization matrix $\overline{\mathbf{C}}$, and $\boldsymbol{\Gamma_{neu}} = \left(\gamma_{neu_1}, \gamma_{neu_2}, \ldots, \gamma_{neu_n}\right)^T$ is the vector of variant-specific neutralization rates, and $\circ$ denotes the Hadamard product.

Thus, given a parameter set $\boldsymbol{\theta}$, DynaVac predicts neutralization titers against 11 pseudoviruses for regimen l as:

$$\widehat{\boldsymbol{NT}}_l(\boldsymbol{\theta}) = \overline{\mathbf{C}}\left(\boldsymbol{\Gamma_{neu}} \circ \boldsymbol{Ab_{lm}}(\boldsymbol{\theta})\right)$$

where $\widehat{\boldsymbol{NT}}_{\boldsymbol{l}}(\boldsymbol{\theta}) = \left(\widehat{NT_{1,l}}(\boldsymbol{\theta}), \widehat{NT_{2,l}}(\boldsymbol{\theta}), \ldots, \widehat{NT_{11,l}}(\boldsymbol{\theta})\right)^{\boldsymbol{T}}$.

For all 29 vaccination regimens, let $\widehat{\boldsymbol{T}}(\boldsymbol{\theta}) = \left(\widehat{T_{i,l}}(\boldsymbol{\theta})\right)_{11\times29}$ be the 11×29 matrix of model-predicted neutralization titers, and let $\boldsymbol{Ab_m}(\boldsymbol{\theta}) = \left(\boldsymbol{Ab_{1m}}(\boldsymbol{\theta}), \boldsymbol{Ab_{2m}}(\boldsymbol{\theta}), \ldots, \boldsymbol{Ab_{29m}}(\boldsymbol{\theta})\right)$ be the corresponding matrix of model-predicted antibody levels at the time of measurement.

Then:

$$\widehat{\boldsymbol{NT}}(\theta) = \overline{\mathbf{C}}[\boldsymbol{\Gamma_{neu}} \boldsymbol{J_{29}} \circ \boldsymbol{Ab_m}(\boldsymbol{\theta})]$$

where $\boldsymbol{J_{29}} = (\mathbf{1}, \mathbf{1}, \ldots, \mathbf{1})_{1\times29}$ is a row vector of ones.

Let $\boldsymbol{NT} = \left(NT_{i,l}\right)_{11\times29}$ be the matrix of experimentally measured neutralization titers.

Define the log2 fold change matrices:

$$\widehat{\boldsymbol{rNT}}(\boldsymbol{\theta}) = \log_2\left(\frac{\widehat{N\boldsymbol{T}}(\boldsymbol{\theta})}{\widehat{NT_{1,1}}(\boldsymbol{\theta})}\right), \ \boldsymbol{rNT} = \log_2\left(\frac{\boldsymbol{NT}}{NT_{1,1}}\right)$$

The objective function L for parameter estimation is the squared Frobenius norm of the difference between the predicted and measured log2 fold change matrices:

$$L(\boldsymbol{\theta}) = |\boldsymbol{rNT} - \widehat{\boldsymbol{rNT}}(\boldsymbol{\theta})|_F^2 \quad (26)$$

The optimization problem is:

$$\boldsymbol{\theta}^* = \arg\min_{\boldsymbol{\theta}} |\boldsymbol{rNT} - \widehat{\boldsymbol{rNT}}(\boldsymbol{\theta})|_F^2, \ \text{subject to } \boldsymbol{lb} \le \boldsymbol{\theta} \le \boldsymbol{ub}$$

where $\boldsymbol{lb}$ and $\boldsymbol{ub}$ are the lower and upper bounds of the prior intervals for each parameter (Supplementary Table 2). The solution $\boldsymbol{\theta}^*$ is the optimal parameter set for the model.

To solve this optimization problem, we employ a genetic algorithm (GA), a heuristic optimization method inspired by natural selection processes. GA iteratively explores the parameter space by encoding parameters as chromosomes, selecting those with better fitness (lower objective function values), and performing genetic operations (mutation, crossover, and selection) to improve solutions[22]. Specifically, the genetic algorithm is implemented using MATLAB's Global Optimization Toolbox function 'ga'. Default settings provided by MATLAB's function were used. The estimated parameter values resulting from optimization based on neutralization titration data from 29 vaccination regimens are provided in Supplementary Table 2.

Appendix for Supplementary Note 2.3: Proof of Theorem

Theorem:

Let $\boldsymbol{Ab} = (Ab_1, Ab_2, ..., Ab_n)^{\boldsymbol{T}}$ be a mixture of antibodies, and let NT_k be the antibody neutralization titer of this mixture against pseudovirus k. Then:

$$NT_k \propto \sum_{j=1}^{n} \gamma_{neu_j} \bar{c}_{k,j} Ab_j = \bar{\boldsymbol{c}}_{\boldsymbol{k}:} \cdot (\boldsymbol{\Gamma_{neu}} \circ \boldsymbol{Ab})$$

where $\bar{\boldsymbol{c}}_{\boldsymbol{k}:}$ represents the k-th row of the matrix $\bar{\mathbf{C}}$, and $\boldsymbol{\Gamma_{neu}} = \left(\gamma_{neu_1}, \gamma_{neu_2}, ..., \gamma_{neu_n}\right)^T$ is the vector of variant-specific neutralization rates.

Proof:

Let $Ka_{i,j}$ be the affinity constant of antibody j (Ab_j) for antigen i (Ag_i). At equilibrium:

$$Ka_{i,j} = \frac{[Ag_i{:}\, Ab_j]}{[Ag_i][Ab_j]}$$

where $[Ag_i{:}\, Ab_j]$ is the concentration of the antibody-antigen complex.

The NT50 titer NT_k is defined as the serum dilution that produces a 50% reduction in the biological effect (pseudovirus infection). For simplicity, we assume that at this dilution, half of the pseudovirus is neutralized:

$$[Ag_k] = \sum_{j=1}^{n} [Ag_k{:}\, Ab_j]$$

and the antibody concentrations are $1/NT_k$ of their initial values.

Equilibrium conditions:

$$\forall j \in \{1,2, ..., n\}, \mathrm{K}a_{k,j} = \frac{[Ag_k{:}\, Ab_j] NT_k}{[Ag_k][Ab_j]}$$

$$NT_k \sum_{j=1}^{n} [Ag_k{:}\, Ab_j] = [Ag_k] \sum_{j=1}^{n} Ka_{k,j} [Ab_j]$$

Solving for T_k:

$$NT_k = \sum_{j=1}^{n} Ka_{k,j} [Ab_j]$$

Expressing $Ka_{k,j}$ in terms of cross-neutralization coefficients and variant-specific neutralization rates according to **Eq.12**:

$$Ka_{k,j} = \bar{c}_{k,j} Ka_j = \frac{\bar{c}_{k,j} \gamma_{neu_j}}{\gamma_c}$$

where γ_c is a constant.

Substituting:

$$NT_k = \frac{1}{\gamma_c} \sum_{j=1}^{n} \bar{c}_{k,j}\, \gamma_{neu_j} [Ab_j] \propto \sum_{j=1}^{n} \gamma_{neu_j} \bar{c}_{k,j} Ab_j = \bar{\boldsymbol{c}}_{\boldsymbol{k}:} \cdot (\boldsymbol{\Gamma_{neu}} \circ \boldsymbol{Ab})$$

This provides a basis for training the model using experimentally measured antibody neutralization titers.

Supplementary Note 3: Model validation using dataset from an independent study

3.1 Parameterization using dataset from an independent study

We collected titration data from another study comprising 37 vaccination regimens in mice involving 4 SARS-CoV-2 strains (Prototype, BA.5, BQ.1.1, and XBB.1.5)[17]. Supplementary Table 18 summarizes the vaccine variant, vaccination time, vaccine type, vaccine amount, serum collection time point, and the geometric mean neutralization titers (GMT) of serum antibodies against the 4 pseudoviruses for each vaccination regimen.

Similarly, we first selected data from the 5 two-dose homologous vaccination regimens (Supplementary Table 9) to estimate the relative proportions of variant-specific neutralization rates γ_{neu_i} (Supplementary Table 10) and the cross-neutralization matrix ($\mathbf{C}$) (Supplementary Table 11).

Using the BA.5-specific neutralization rate γ_{neu}^{BA5} as a reference, define the relative ratios $f_i^{BA5} = \frac{T_{i,i}}{T_{BA5,BA5}} = \frac{\gamma_{neu,i}}{\gamma_{neu}^{BA5}}$. For the protein vaccines (BA.5, BQ.1.1, XBB.1.5) administered at 10 μg, the relative ratio can be calculated directly. The ratio for CoronaVac $\left(f_{CoronaVac}^{\mathrm{BA5}}\right)$ and wild type mRNA vaccine $\left(f_{mRNA}^{\mathrm{BA5}}\right)$ cannot be directly inferred because the vaccine types and doses differ. Therefore, $f_{CoronaVac}^{\mathrm{BA5}}$ and f_{mRNA}^{BA5} are set as unknown parameters in the Yisimayi, et al. dataset.

The estimated parameter values obtained by training on the titration data of the 37 vaccination regimens in Yisimayi, et.al. dataset using genetic algorithm following the same procedure in Supplementary Note 2.3 are shown in Supplementary Table 2.

3.2 Cross-dataset validation

We used the genetic algorithm to jointly train a complete set of model parameters on both our dataset and the Yisimayi, et al. dataset, as shown in Supplementary Table 2. The loss function used for training was the sum of the loss functions defined by **Equation. 26** for the two datasets. When performing cross-dataset predictions, for the primary parameters shared between the two datasets, we directly applied the values trained on the parameterization dataset to the validation dataset. For parameters unique to either dataset (those marked with superscripts a or b in Supplementary Table 2), we utilized the values trained on the combined dataset.

Supplementary Note 4: Variance contributions calculation

To quantify the relative importance of different antigenic distances ($d_{0,2}$and $d_{1,2}$) in determining neutralization responses, we employed variance-based sensitivity analysis using the Sobol method. For each parameter, the first-order Sobol index (variance contribution rate, S_i) was calculated as:

$$S_i = \frac{V_{x_i}\left[E_{x_{-i}}(y|x_i)\right]}{V(y)}$$

where $V(y)$ represents the total variance of the neutralization output across all parameter combinations, $E_{x_{-i}}(y|x_i)$denotes the expected value of neutralization when parameter x_i is fixed, and $V_{x_i}[\cdot]$ is the variance of this conditional expectation across different values of x_i.

Computationally, we calculated the total variance ($V(y)$) of all neutralization values, then for each parameter (e.g., $d_{0,2}$), computed mean neutralization responses along each fixed value while varying the other parameter (e.g., $d_{1,2}$). The variance of these conditional means was then normalized by the total variance to obtain the variance contribution rate. The remaining variance ($1 - S_1 - S_2$) was attributed to the interaction term S_{12}

Supplementary Note 5: Simulation Framework for DynaVac-Guided Vaccination Strategy Optimization Against Antigenically Evolving Pathogens

5.1 Antigenic Drift Simulation

To simulate the evolutionary dynamics of a mutable virus ("Pathogen X"), we modeled antigenic drift as a stochastic Poisson process in a one-dimensional antigenic space. Drift events occur as discrete one-unit shifts in antigenic coordinates at exponentially distributed time intervals:

$$\Delta t_i \sim \text{Exponential}(\lambda), \quad t_k = \sum_{i=1}^{k} \Delta t_i \tag{27}$$

Where $\lambda \in \{0.1,\ 0.3,\ 0.5\}$ (antigenic distance units/month) denotes the average rate of antigenic drift, corresponding to slow, moderate, or fast mutational dynamics, respectively. The cumulative number of drift events up to time t defines the position in antigenic space:

$$A(t) = \max\{k | t_k \leq t\} \tag{28}$$

which we refer to as the antigenic coordinate of the circulating strain at time t. The antigenic distance between circulating strain at any two timepoints t_i and t_j is then given by the Euclidean distance in this space:

$$D_{i,j} = \left|A(t_i) - A(t_j)\right| \tag{29}$$

This setup enables stochastic yet biologically interpretable simulation of pathogen evolution over a continuous timeline. For each simulation (100 runs per λ), we tracked monthly antigenic positions over a 75-month horizon.

5.2 Vaccination Strategies Simulation

For each simulated antigenic drift, we evaluated four empirical strategies (with updates every 6, 12, 18, or 24 months) and one model-guided strategy (DynaVac), in which vaccine updates were triggered upon entry into the immune-imprinting breakthrough zone, defined based on the antigenic distance–interval phase-plane (Fig. 7b, main text). Each update consisted of two 30 μg mRNA doses spaced one month apart, using the circulating antigenic variant at the time of update as the vaccine strain.

Immune responses were simulated using the DynaVac model (**Equations 20–24**, Supplementary Note 2.2) with the human-data-trained parameter set (Supplementary Table 2), tracking the time evolution of antigen levels, naive and memory B cell populations, and antibody levels specific to each antigenic variant.

5.3 Protection Metric

To evaluate protective immunity, we first defined the neutralization efficacy against the circulating strain A(t) at time t as:

$$T(t) = \sum_{i=1}^{n} Ab_i(t) \cdot 2^{-D_{i,A(t)}} \tag{30}$$

which accounts for both homologous and cross-reactive antibody contributions; $Ab_i(t)$ is the variant i specific antibody level at time t, and $D_{i,A(t)}$ is the antigenic distance between that variant i and the circulating strain at time t.

The overall protection (OP) of a given strategy was computed as the time-averaged log10-neutralization from month 1 to 75:

$$\text{OP} = \frac{1}{T - t_0} \int_{t_0}^{T} \log_{10} T\,(t)\, dt \quad \text{with } t_0 = 1,\ T = 75 \tag{31}$$

To enable comparison across strategies with differing update frequencies, we also computed:

$$\mathrm{OP}_{\text{per update}} = \frac{\mathrm{OP}}{n_{\text{updates}}}$$

where n_{updates} is the number of vaccine updates, each consisting of two doses.

Reference

1 Miller, F. J. Immunobiology: The Immune System in Health and Disease. Charles A. Janeway, Jr. , Paul Travers , Mark Walport , J. Donald Capra. *The Quarterly Review of Biology* **75**, 224-225 (2000).

2 Roth, D. B. & Craig, N. L. VDJ recombination: a transposase goes to work. *Cell* **94**, 411-414, doi:10.1016/s0092-8674(00)81580-9 (1998).

3 Tonegawa, S. Somatic generation of antibody diversity. *Nature* **302**, 575-581, doi:10.1038/302575a0 (1983).

4 Victora, G. D. & Nussenzweig, M. C. Germinal centers. *Annu Rev Immunol* **30**, 429-457, doi:10.1146/annurev-immunol-020711-075032 (2012).

5 Di Noia, J. M. & Neuberger, M. S. Molecular mechanisms of antibody somatic hypermutation. *Annu Rev Biochem* **76**, 1-22, doi:10.1146/annurev.biochem.76.061705.090740 (2007).

6 Victora, G. D. & Mesin, L. Clonal and cellular dynamics in germinal centers. *Curr Opin Immunol* **28**, 90-96, doi:10.1016/j.coi.2014.02.010 (2014).

7 Cohen, J. J., Duke, R. C., Fadok, V. A. & Sellins, K. S. Apoptosis and Programmed Cell Death in Immunity. *Annual Review of Immunology* **10**, 267-293, doi:10.1146/annurev.iy.10.040192.001411 (1992).

8 Eisen, H. N. & Siskind, G. W. VARIATIONS IN AFFINITIES OF ANTIBODIES DURING THE IMMUNE RESPONSE. *Biochemistry* **3**, 996-1008, doi:10.1021/bi00895a027 (1964).

9 Suan, D., Sundling, C. & Brink, R. Plasma cell and memory B cell differentiation from the germinal center. *Curr Opin Immunol* **45**, 97-102, doi:10.1016/j.coi.2017.03.006 (2017).

10 Kurosaki, T., Kometani, K. & Ise, W. Memory B cells. *Nat Rev Immunol* **15**, 149-159, doi:10.1038/nri3802 (2015).

11 Inoue, T. & Kurosaki, T. Memory B cells. *Nature Reviews Immunology* **24**, 5-17, doi:10.1038/s41577-023-00897-3 (2024).

12 Dogan, I. *et al.* Multiple layers of B cell memory with different effector functions. *Nature Immunology* **10**, 1292-1299, doi:10.1038/ni.1814 (2009).

13 Pape, K. A. & Jenkins, M. K. Do Memory B Cells Form Secondary Germinal Centers? It Depends. *Cold Spring Harbor perspectives in biology* **10**, doi:10.1101/cshperspect.a029116 (2018).

14 Mesin, L. *et al.* Restricted Clonality and Limited Germinal Center Reentry Characterize Memory B Cell Reactivation by Boosting. *Cell* **180**, 92-106.e111, doi:10.1016/j.cell.2019.11.032 (2020).

15 Moran, I., Grootveld, A. K., Nguyen, A. & Phan, T. G. Subcapsular Sinus Macrophages: The Seat of Innate and Adaptive Memory in Murine Lymph Nodes. *Trends in Immunology* **40**, 35-48, doi:https://doi.org/10.1016/j.it.2018.11.004 (2019).

16 Moran, I. *et al.* Memory B cells are reactivated in subcapsular proliferative foci of lymph nodes. *Nature communications* **9**, 3372, doi:10.1038/s41467-018-05772-7 (2018).

17 Yisimayi, A. *et al.* Repeated Omicron exposures override ancestral SARS-CoV-2 immune imprinting. *Nature* **625**, 148-156, doi:10.1038/s41586-023-06753-7 (2024).

18 Koutsakos, M. & Ellebedy, A. H. Immunological imprinting: Understanding COVID-19. *Immunity* **56**, 909-913, doi:10.1016/j.immuni.2023.04.012 (2023).

19 Hu, Y. F. *et al.* Rational design of a booster vaccine against COVID-19 based on antigenic distance. *Cell host & microbe* **31**, 1301-1316.e1308, doi:10.1016/j.chom.2023.07.004 (2023).

20 Rössler, A., Knabl, L., von Laer, D. & Kimpel, J. Neutralization Profile after Recovery from SARS-CoV-2 Omicron Infection. *The New England journal of medicine* **386**, 1764-1766, doi:10.1056/NEJMc2201607 (2022).

21 Pan, K. Understanding original antigenic sin in influenza with a dynamical system. *PloS one* **6**, e23910, doi:10.1371/journal.pone.0023910 (2011).

22 Mitchell, M.

23 Whitley, D. A genetic algorithm tutorial. *Statistics and Computing* **4**, 65-85, doi:10.1007/BF00175354 (1994).

24 Olofsson, S. O. *et al.* Structure and biosynthesis of apolipoprotein B. *Am Heart J* **113**, 446-452, doi:10.1016/0002-8703(87)90612-0 (1987).

25 Schwalb, B. *et al.* TT-seq maps the human transient transcriptome. *Science* **352**, 1225-1228, doi:10.1126/science.aad9841 (2016).

26 Padovan-Merhar, O. *et al.* Single mammalian cells compensate for differences in cellular volume and DNA copy number through independent global transcriptional mechanisms. *Mol Cell* **58**, 339-352, doi:10.1016/j.molcel.2015.03.005 (2015).
27 Lee, H. Y. *et al.* Simulation and prediction of the adaptive immune response to influenza A virus infection. *J Virol* **83**, 7151-7165, doi:10.1128/jvi.00098-09 (2009).
28 Hogan, A. B. *et al.* Estimating long-term vaccine effectiveness against SARS-CoV-2 variants: a model-based approach. *Nature Communications* **14**, 4325, doi:10.1038/s41467-023-39736-3 (2023).
29 Ndifon, W. A simple mechanistic explanation for original antigenic sin and its alleviation by adjuvants. *J R Soc Interface* **12**, doi:10.1098/rsif.2015.0627 (2015).
30 Bocharov, G. A. & Romanyukha, A. A. Mathematical model of antiviral immune response. III. Influenza A virus infection. *J Theor Biol* **167**, 323-360, doi:10.1006/jtbi.1994.1074 (1994).
31 Raman, C. S., Jemmerson, R., Nall, B. T. & Allen, M. J. Diffusion-limited rates for monoclonal antibody binding to cytochrome c. *Biochemistry* **31**, 10370-10379, doi:10.1021/bi00157a027 (1992).
32 Hancioglu, B., Swigon, D. & Clermont, G. A dynamical model of human immune response to influenza A virus infection. *J Theor Biol* **246**, 70-86, doi:10.1016/j.jtbi.2006.12.015 (2007).

Extended Data Figures

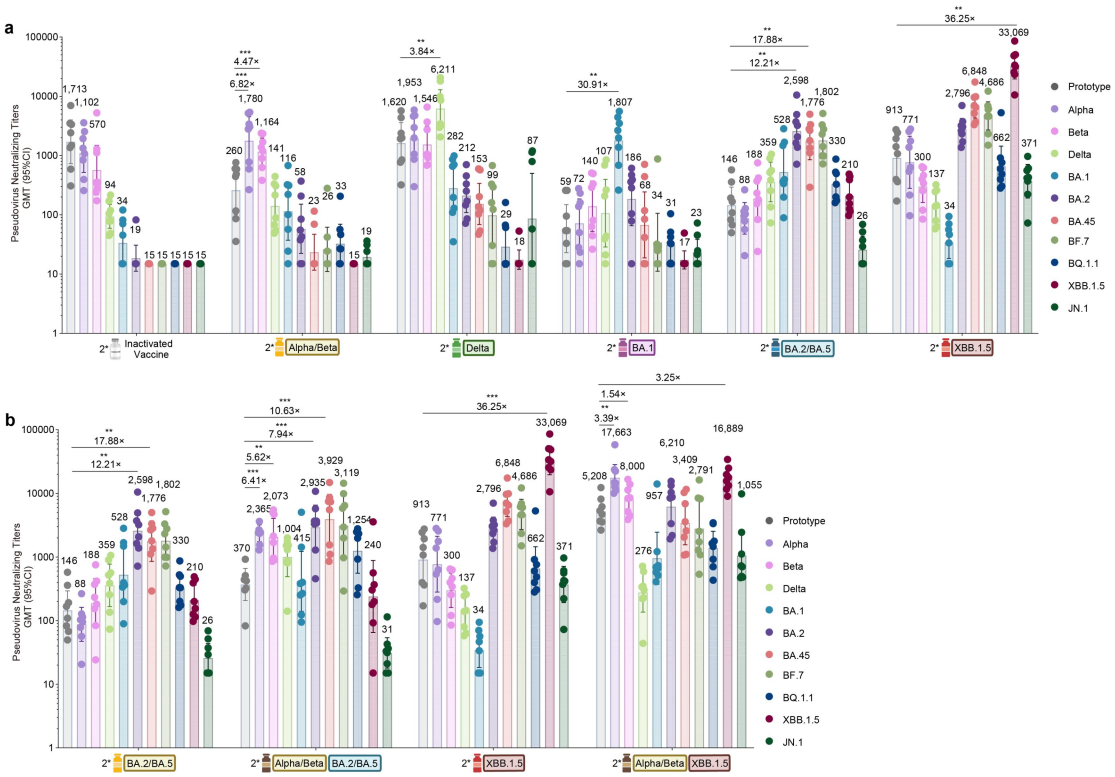

Extended Data Fig. 1 Pseudovirus assay of mice sera that received two-dose variant vaccination

a, b, Neutralization titers against 11 SARS-CoV-2 variants of C57BL/6J mice sera that received two-dose variant mRNA vaccine. The antigen components of different groups of vaccines are directly marked below. All the experimental mice were divided into 8 groups according to the type of booster vaccination, each group contains 8 mice. The neutralization titers were expressed as 50% neutralizing titer (NT50). Geometric mean titer (GMT) values were marked on top of bars. Each dot represents the result of one mouse serum sample, geometric mean ratio (GMR) and *P* values were marked above corresponding bars. Data are presented as the geometric mean titers with 95% confidence intervals. Specific details were shown in Supplementary Table 14.
$^{**}P < 0.01$; $^{***}P < 0.001$ (two-tailed student's *t*-test in (**a-b**))

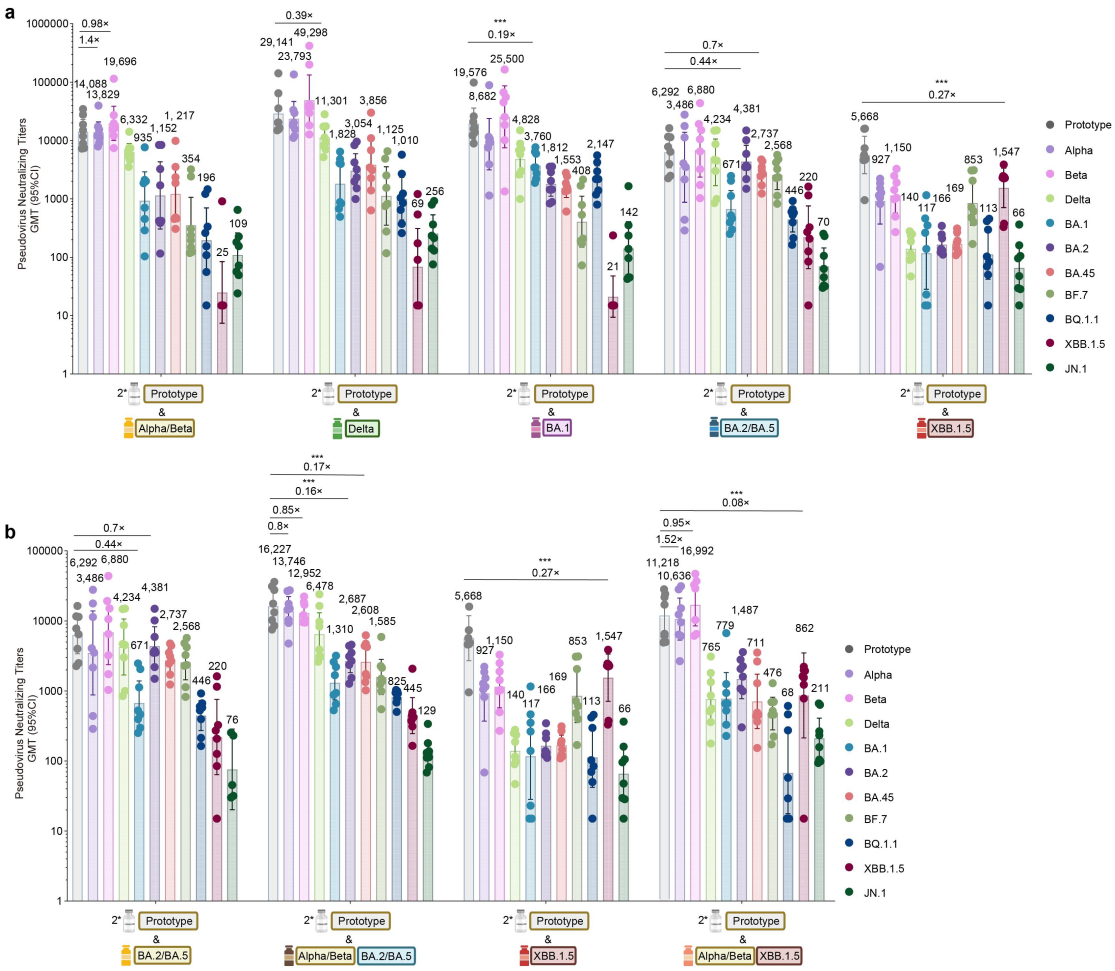

Extended Data Fig. 2 Pseudovirus assay of mice sera that received one-dose booster based on two-dose inactivated vaccines

a, b, Neutralization titers against 11 SARS-CoV-2 variants of C57BL/6J mice sera that received one-dose variant booster based on two-dose inactivated vaccines. The antigen components of vaccines are directly marked below. All the experimental mice were divided into 7 groups according to the type of variant booster, each group contains 8 mice. The neutralization titers were expressed as 50% neutralizing titer (NT50). Geometric mean titer (GMT) values were marked on top of bars. Each dot represents the result of one mouse serum sample, geometric mean ratio (GMR) and *P* values were marked above corresponding bars. Data are presented as the geometric mean titers with 95% confidence intervals. Specific details were shown in Supplementary Table 15.

***$P < 0.001$ (two-tailed student's *t*-test in (**a-b**))

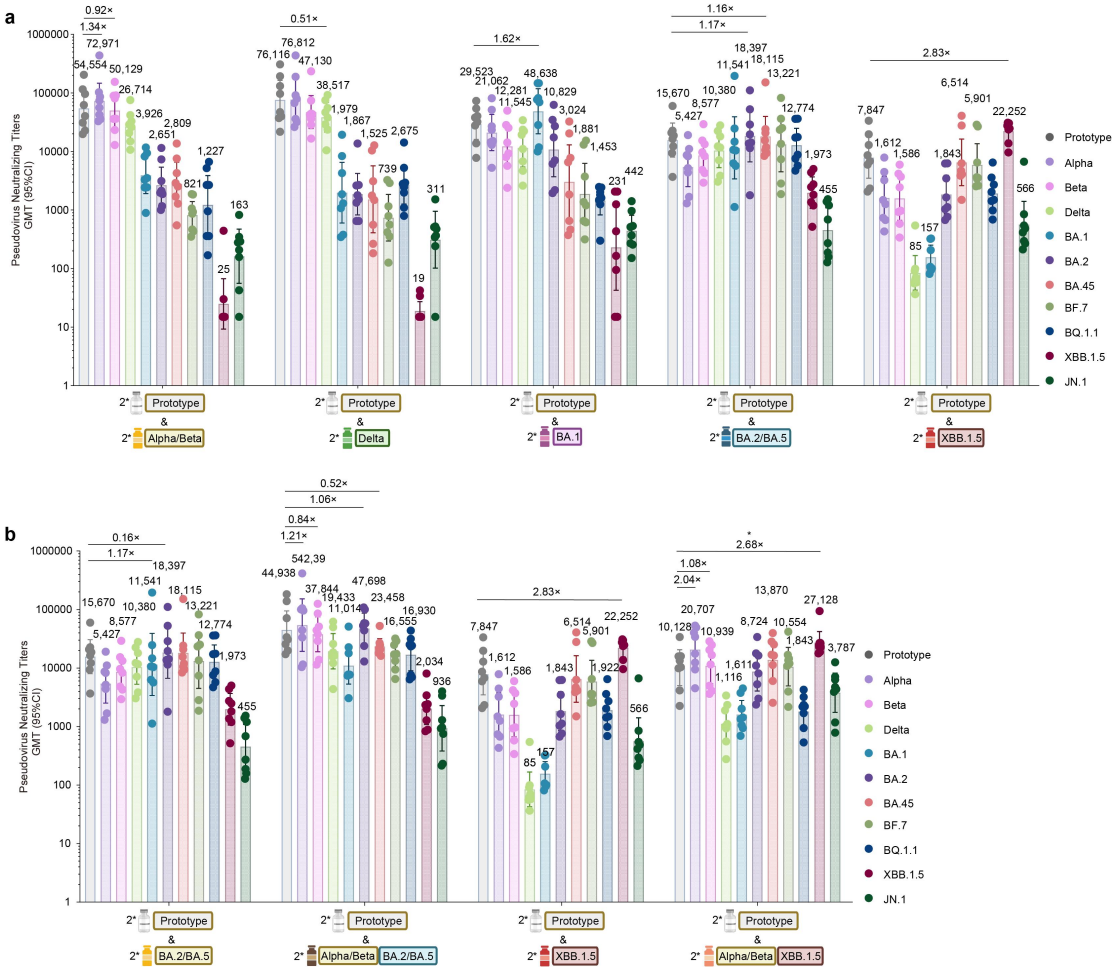

Extended Data Fig. 3 Pseudovirus assay of mice sera that received two-dose boosters based on two-dose inactivated vaccines

a, b, Neutralization titers against 11 SARS-CoV-2 variants of C57BL/6J mice sera that received two-dose variant boosters based on two-dose inactivated vaccines. The antigen components of vaccines are directly marked below. All the experimental mice were divided into 7 groups according to the type of variant booster, each group contains 8 mice. The neutralization titers were expressed as 50% neutralizing titer (NT50). Geometric mean titer (GMT) values were marked on top of bars. Each dot represents the result of one mouse serum sample, geometric mean ratio (GMR) and *P* values were marked above corresponding bars. Data are presented as the geometric mean titers with 95% confidence intervals. Specific details were shown in Supplementary Table 16.

*$P < 0.05$ (two-tailed student's *t*-test in (**a-b**))

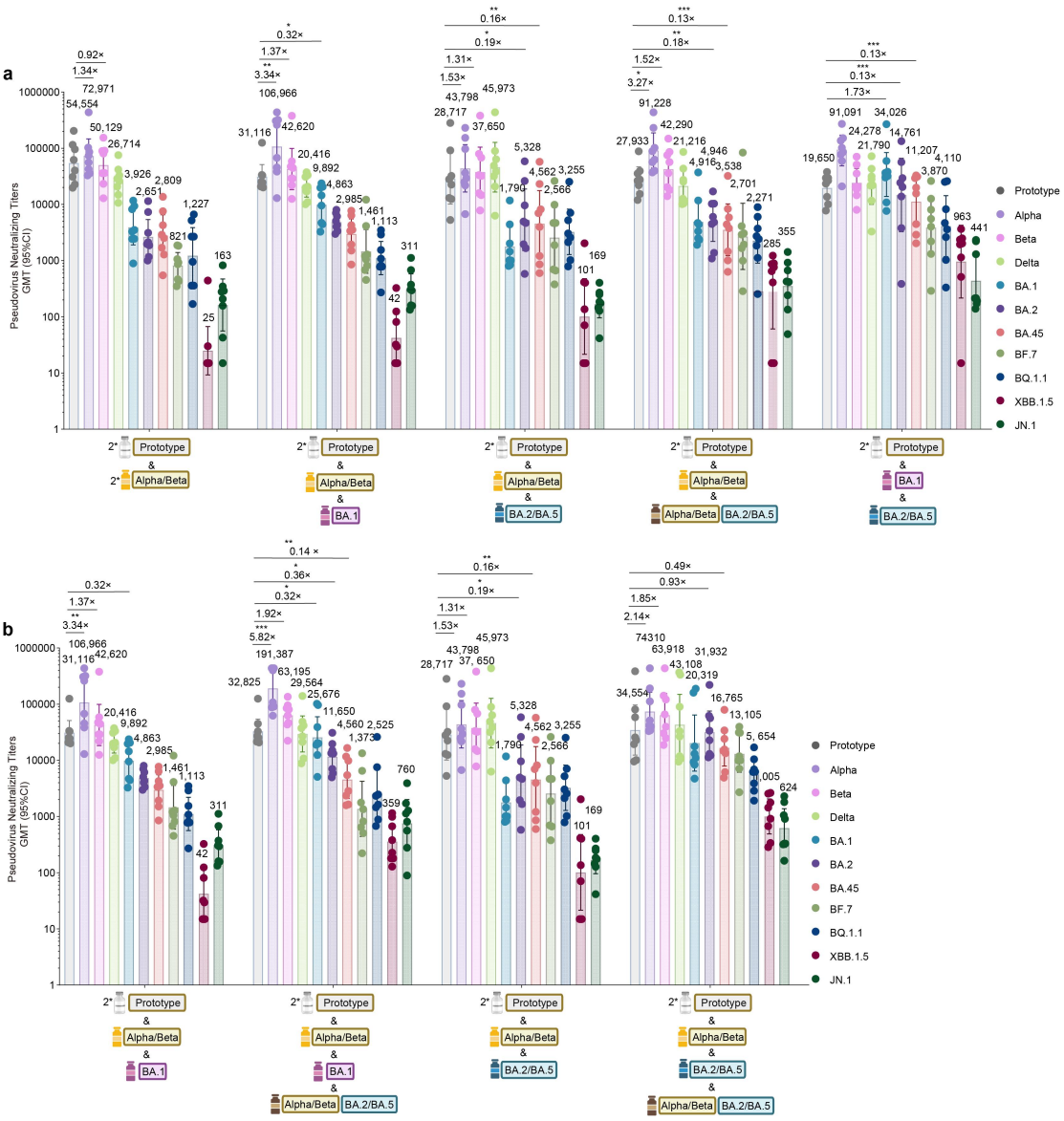

Extended Data Fig. 4 Pseudovirus assay of mice sera that received different one or two -dose variant boosters based on two-dose inactivated vaccines and one-dose Alpha/Beta vaccine

a, b, Neutralization titers against 11 SARS-CoV-2 variants of C57BL/6J mice sera that received two-dose inactivated vaccines followed by progressively sequential variant booster regimens. The antigen components of vaccines are directly marked below. All the experimental mice were divided into 7 groups according to the type of variant booster, each group contains 8 mice. The neutralization titers were expressed as 50% neutralizing titer (NT50). Geometric mean titer (GMT) values were marked on top of bars. Each dot represents the result of one mouse serum sample, geometric mean ratio (GMR) and *P* values were marked above corresponding bars. Data are presented as the geometric mean titers with 95% confidence intervals. Specific details were shown in Supplementary Table 17.

P* < 0.05; ***P* < 0.01; ****P* < 0.001 (two-tailed student's *t*-test in (a-b**))

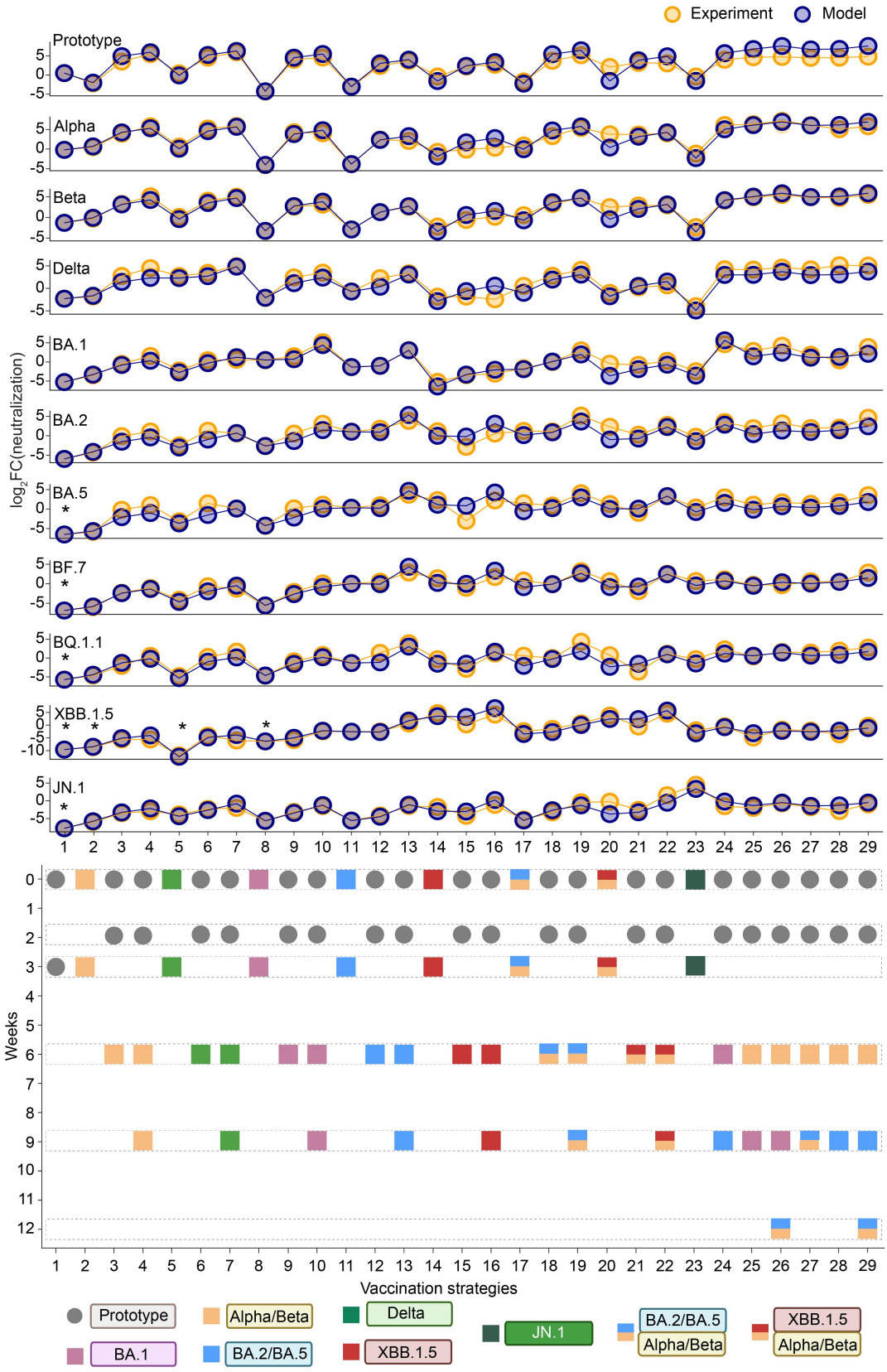

Extended Data Fig. 5 Comparison of experimentally measured and DynaVac-fitted neutralization titers in our mouse study

Scatter plot showing log2 fold changes of neutralization titers for 29 vaccination regimens (columns) against 11 SARS-CoV-2 variants (rows), relative to neutralization titer against the prototype strain after two doses of inactivated vaccines. Experimental data (orange) were used for

model parameterization, and model-predicted values are shown in purple. Asterisks indicate data points corrected by the model due to experimental assay detection limits. Bottom panel depicts detailed vaccination schedules (gray circles: inactivated vaccines; colored squares: monovalent mRNA vaccines; mixed-color squares: bivalent vaccines).

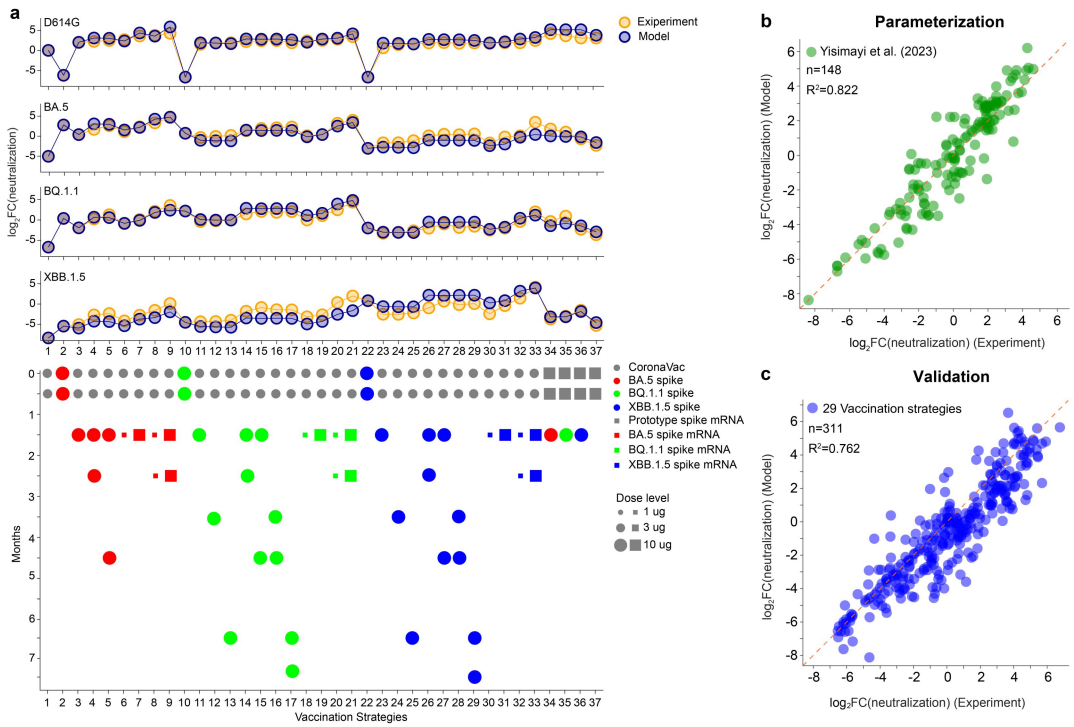

Extended Data Fig. 6 Parameterization of the DynaVac model using Yisimayi et al. (2023) mouse data and cross-dataset validation

a, Comparison of experimentally measured (orange) and DynaVac-fitted (purple) neutralization titers after parameterization using the Yisimayi et al. (2023) dataset. Scatter plot shows log2 fold changes of neutralization titers for 37 vaccination regimens (columns) against 4 SARS-CoV-2 variants (rows), relative to neutralization titer against the D614G strain after two doses of inactivated vaccines. Bottom panel shows detailed vaccination schedules (gray circles: inactivated vaccines; gray squares: prototype spike mRNA vaccines; colored dots/squares: spike or mRNA vaccines; size of dots/squares indicates dose level).

b, Performance of the DynaVac model parameterized on the Yisimayi et al. (2023) dataset. Scatter plot shows predicted versus observed log2 neutralization titer fold changes for the parameterization dataset. R^2 value represents the proportion of variability in the observed data accounted for by model predictions.

c, Cross-dataset validation of the DynaVac model parameterized on the Yisimayi et al. (2023) dataset and validated using our mouse study dataset. Scatter plot shows predicted versus observed log2 neutralization titer fold changes. R^2 value represents the proportion of variability in the observed data accounted for by model predictions.

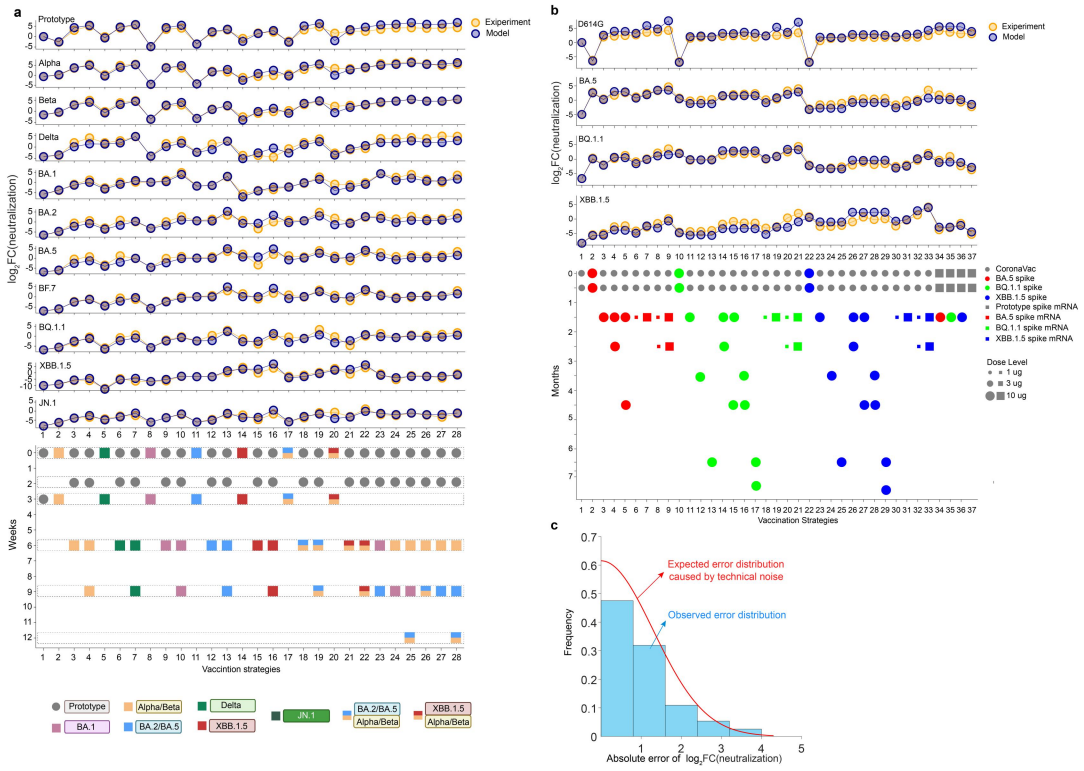

Extended Data Fig. 7 Comparison of experimentally measured and DynaVac-fitted neutralization titers after parameterization using the combined mouse dataset

a, Comparison of experimentally measured (orange) and DynaVac-fitted (purple) neutralization titers for our mouse study after parameterization using the combined dataset. Scatter plot shows log2 fold changes of neutralization titers for 28 vaccination regimens (columns) against 11 SARS-CoV-2 variants (rows), relative to neutralization titer against the prototype strain after two doses of inactivated vaccines. Bottom panel depicts detailed vaccination schedules (gray circles: inactivated vaccines; colored squares: monovalent mRNA vaccines; mixed-color squares: bivalent vaccines).

b, Comparison of experimentally measured (orange) and DynaVac-fitted (purple) neutralization titers for the Yisimayi et al. (2023) dataset after parameterization using the combined dataset. Scatter plot shows log2 fold changes of neutralization titers for 37 vaccination regimens (columns) against 4 SARS-CoV-2 variants (rows), relative to neutralization titer against the D614G strain after two doses of inactivated vaccines. Bottom panel shows detailed vaccination schedules (gray circles: inactivated vaccines; gray squares: prototype spike mRNA vaccines; colored dots/squares: Omicron sub-variant spike or mRNA vaccines; size of dots/squares indicates dose level).

c, Error distribution of the DynaVac model parameterized on the combined mouse dataset. Histogram shows the distribution of absolute errors in log2 neutralization titer fold change predictions. Red line represents a half-normal distribution with $\sigma = 1.3$ fitted to the error distribution.

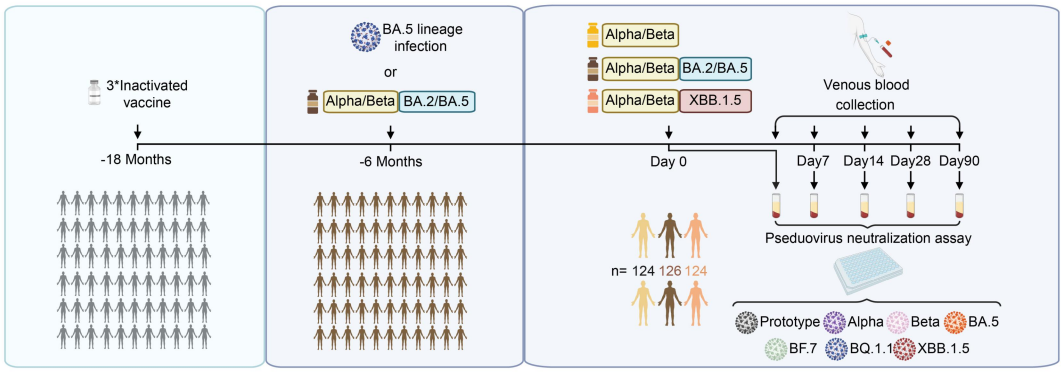

668
669 **Extended Data Fig. 8 Schematic representation of the human clinical trial**
670 Pseudovirus neutralization assay of human sera from 3 vaccination regimens (376 volunteers).
671 Volunteers who accepted three-dose inactivated vaccines and one-dose BA.2/BA.5+Alpha/Beta
672 vaccine (or infected with BA.5.2/BF.7 variant) were randomly divided into three groups. Each
673 group accepted one of mRNA variant boosters (Alpha/Beta vaccine, BA.2/BA.5+Alpha/Beta
674 vaccine, or XBB.1.5+Alpha/Beta vaccine). Pseudovirus neutralization titers of volunteer serum
675 samples were tested against 7 SARS-CoV-2 variants.

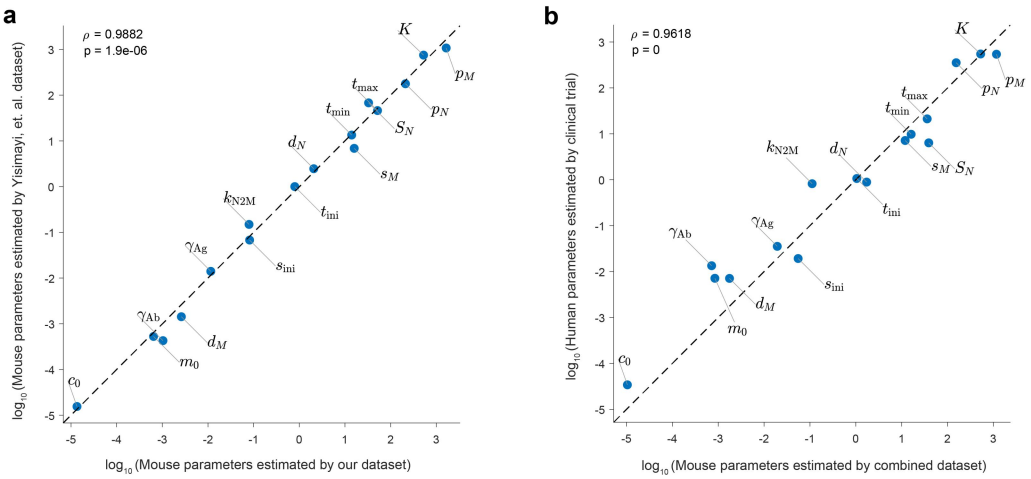

Extended Data Fig. 9 Log-transformed immunodynamic parameter comparisons across datasets and species.

a, Comparison of log-transformed parameter values inferred from our mouse dataset (x-axis) and those from Yisimayi et al. dataset (y-axis). Each dot represents a fitted immunological parameter with symbol definitions detailed in Supplementary Table 2. The dashed line denotes the identity line (x = y).

b, Comparison of parameter values inferred from the combined mouse dataset (x-axis) and the human dataset (y-axis). Each dot corresponds to a model parameter with symbol definitions detailed in Supplementary Table 2. The dashed line denotes the identity line. Spearman correlation coefficients (ρ) and associated P values are shown in each panel.

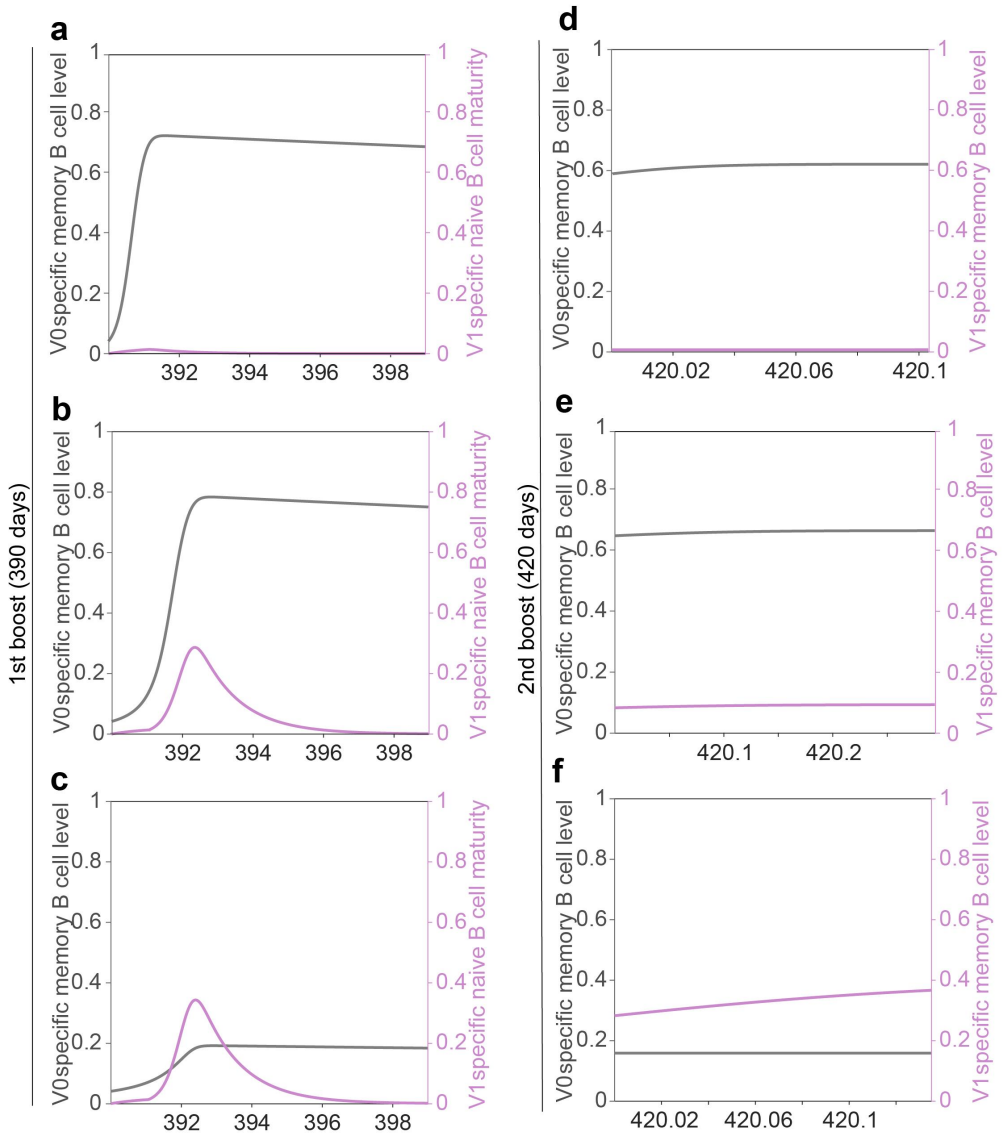

Extended Data Fig. 10 Dynamics of prototype-specific and variant-specific B cell responses over time following booster vaccinations

a-c, Comparison of prototype-specific memory B cells (V_0, gray) and variant-specific naive B cells maturity (V_1, purple) after the first vaccination administered at day 390 for prime-boost antigenic distance of 1.6 (**a**, immune-imprinting-protection zone), 5.0 (**b**, immune-imprinting-pitfall zone), and 5.6 (**c**, immune-imprinting-breakthrough zone).

d-f, Comparison of prototype-specific memory B cells (V_0, gray) and variant-specific memory B cells (V_1, purple) after the second booster vaccination administered at day 420 for prime-boost antigenic distance of 1.6 (**d**, immune-imprinting-protection zone), 5.0 (**e**, immune-imprinting-pitfall zone), and 5.6 (**f**, immune-imprinting-breakthrough zone).

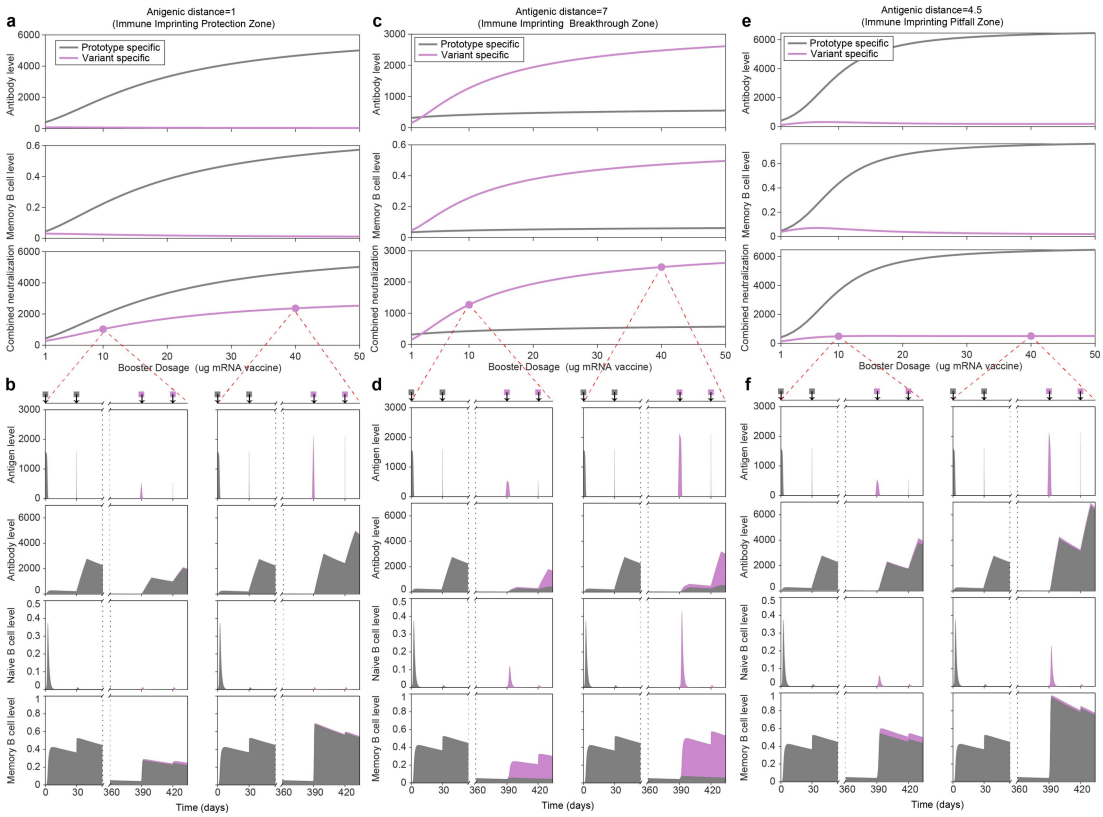

Extended Data Fig. 11 The effect of booster dose on the dynamics of humoral immune response and immune imprinting at different antigenic distances

a, c, e, Continuous relationship between immune imprinting effect and booster dose for prime-boost antigenic distance of 1.0 (**a**, immune-imprinting-protection zone), 7.0 (**c**, immune-imprinting-breakthrough zone), and 4.5 (**e**, immune-imprinting-pitfall zone). The top panel shows the antibody levels specific to prototype (gray line) and variant (purple line) on day 434 (2 weeks after the second booster dose) as a function of booster dose. The middle panel shows the corresponding memory B cell levels as a function of booster dose. The bottom panel displays the combined neutralization against the variant, which is composed of cross-neutralization attributed to prototype-specific antibodies and direct-neutralization from variant-specific antibodies. **b, d, f,** Dynamics of key humoral immunity components during the evolution of immunogenicity in varying booster dose scenarios for prime-boost antigenic distance of 1.0 (**b**, immune-imprinting-protection zone), 7.0 (**d**, immune-imprinting-breakthrough zone), and 4.5 (**f**, immune-imprinting-pitfall zone). Each row shows the dynamics of antigen level, naive B cell gross affinity (maturity), memory B cell level, and antibody level over time. The gray areas represent prototype-specific quantities while the purple areas represent variant-specific quantities. The left column represents scenarios with a booster dose of 10 μg, while the right column represents scenarios with a booster dose of 40 μg.

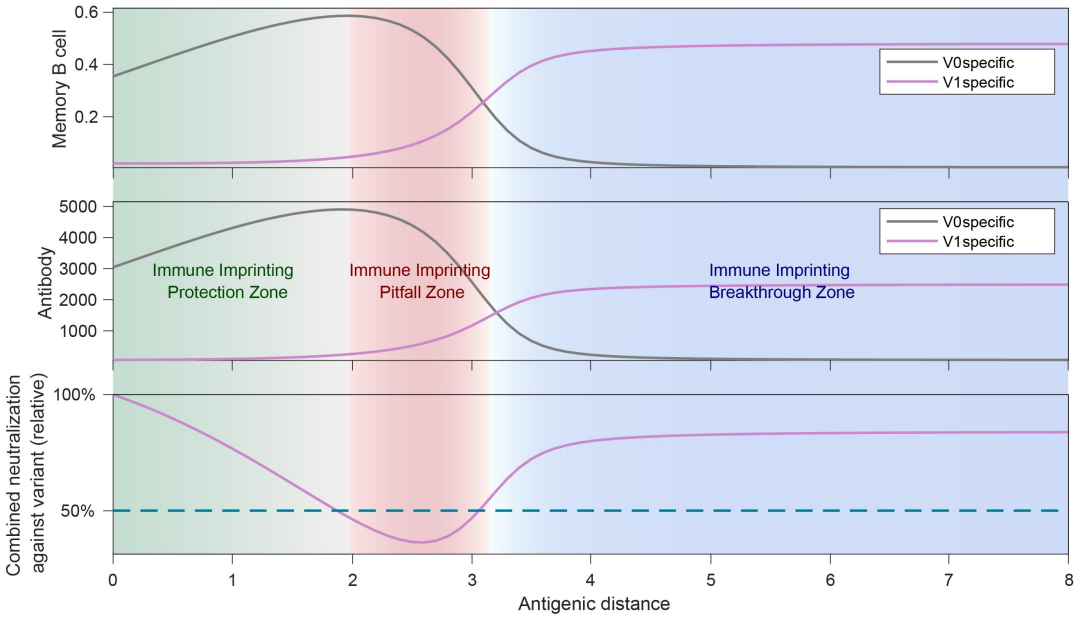

Extended Data Fig. 12 Continuous relationship between immune imprinting effect and antigenic distance under weak primary immunization (3 μg)

The top panel shows the antibody levels specific to the prototype (gray line) and the variant (purple line) on day 434 (2 weeks after the second booster dose). The middle panel shows the corresponding memory B cell levels. The bottom panel displays the relative combined neutralization against the variant, which combines cross-neutralization from prototype-specific antibodies and direct-neutralization from variant-specific antibodies, relative to the neutralization at an antigenic distance of 0 (i.e., no antigenic drift). The cyan dashed line indicates the 50% threshold, which divides the antigenic distance into three zones: the immune-imprinting-protection zone (green background, relative neutralization ≥50% on the left side of the nadir); the immune-imprinting-pitfall zone (red background, relative neutralization <50%); and the immune-imprinting-breakthrough zone (blue background, relative neutralization ≥50% on the right side of the nadir).

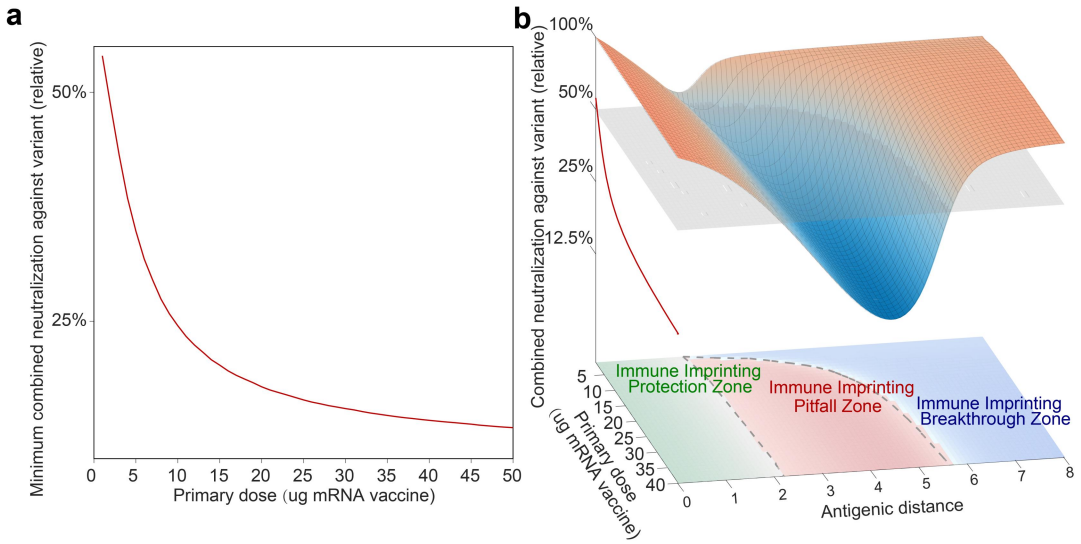

Extended Data Fig. 13 Impact of primary immunization strength on the depth of immune-imprinting-pitfall zone

a, The relationship between primary dose and the lowest combined neutralization against variant (relative) within the immune-imprinting-pitfall zone.

b, The 3D surface showing the interplay between primary dose, prime-boost antigenic distance and their synthetic effect on the combined neutralization against variant. The surface is divided into three immune-imprinting zones defined by the antigenic distance. The red curve represents the projection of the lowest combined neutralization against variant (relative) within the immune-imprinting-pitfall zone for each primary dose onto the primary dose-combined neutralization plane. This projection corresponds to the same scenario illustrated in (**a**).

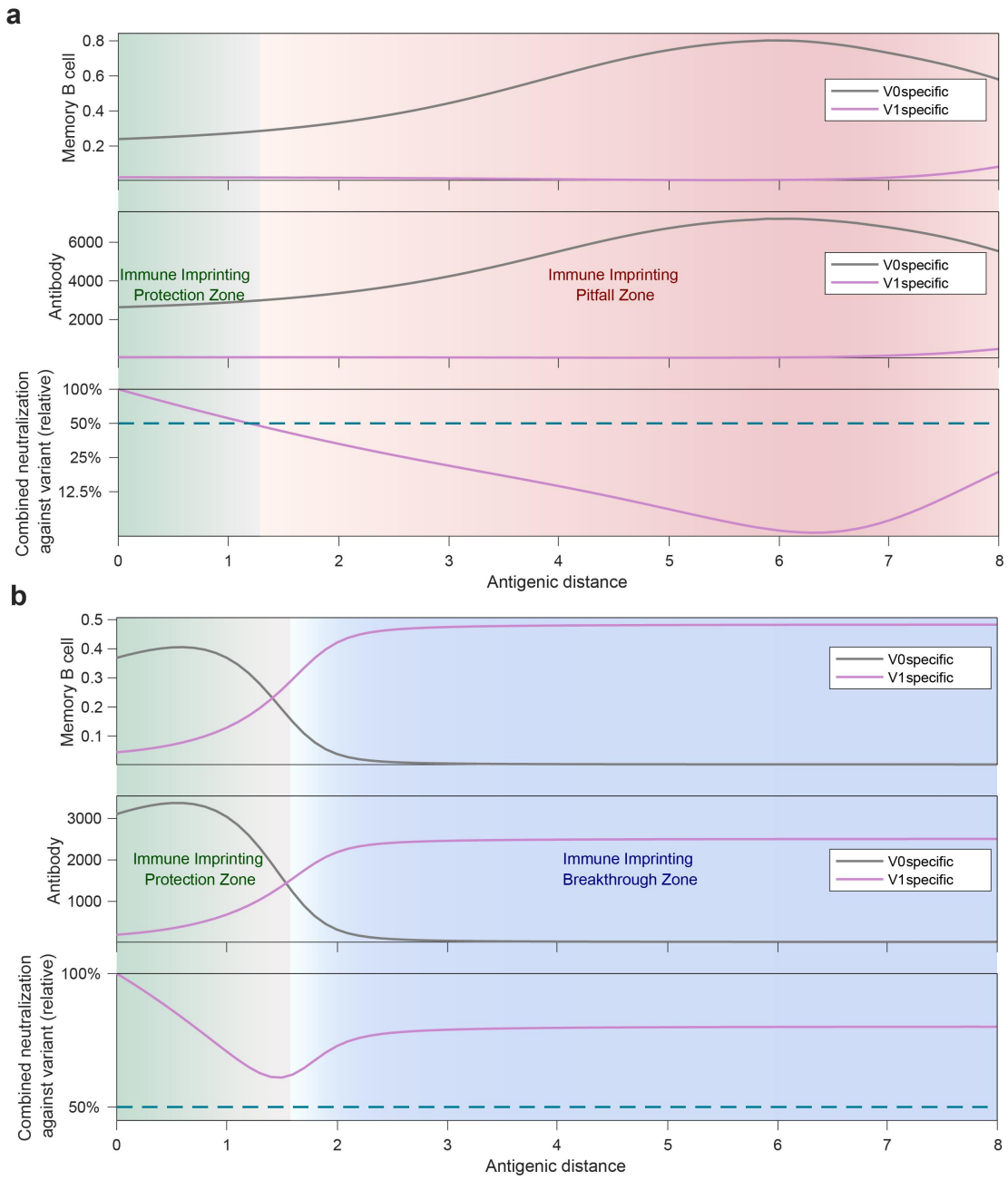

Extended Data Fig. 14 Continuous relationship between immune imprinting effect and antigenic distance under shortened and lengthened prime-boost intervals

a, b, The prime-booster intervals were set as 3 months (**a**) and 24 months (**b**), respectively. The top panel shows the antibody levels specific to the prototype (gray line) and the variant (purple line) on day 434 (2 weeks after the second booster dose). The middle panel shows the corresponding memory B cell levels. The bottom panel displays the relative combined neutralization against the variant, which combines cross-neutralization from prototype-specific antibodies and direct-neutralization from variant-specific antibodies, relative to the neutralization at an antigenic distance of 0 (i.e., no antigenic drift). The cyan dashed line indicates the 50% threshold, which divides the antigenic distance into three zones: the immune-imprinting-protection zone (green background, relative neutralization ≥50% on the left side of the nadir); the immune-imprinting-pitfall zone (red background, relative neutralization <50%); and the immune-imprinting-breakthrough zone (blue background, relative neutralization ≥50% on the right side of the nadir).

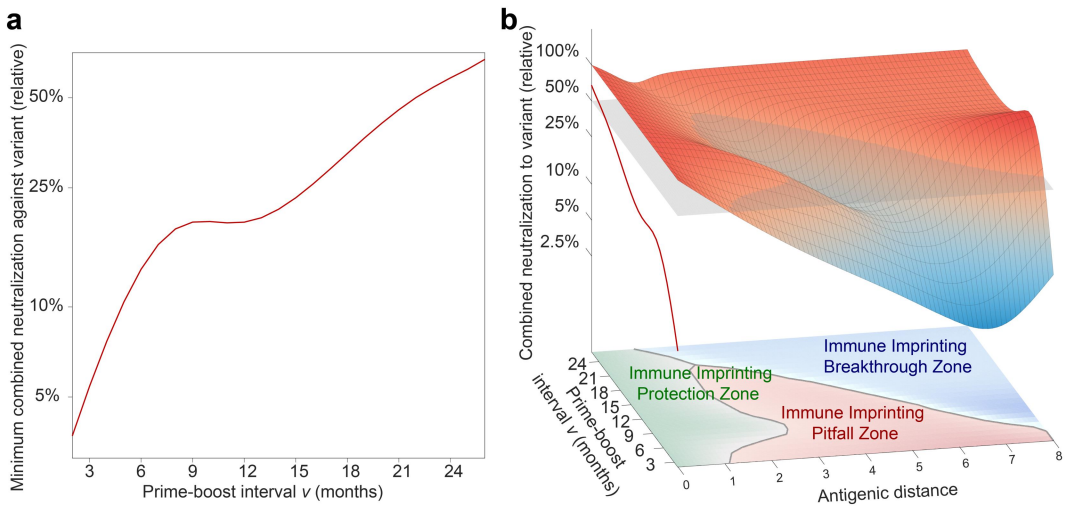

Extended Data Fig. 15 Impact of prime-boost interval on the depth of immune-imprinting-pitfall zone

a, The relationship between prime-boost interval and the minimum combined neutralization against variant (relative) within the immune-imprinting-pitfall zone.

b, The 3D surface showing the interplay between prime-booster interval, prime-boost antigenic distance and their synthetic effect on the combined neutralization against variant. The surface is divided into three immune-imprinting zones defined by the antigenic distance. The red curve represents the projection of the lowest combined neutralization against variant (relative) within the immune-imprinting-pitfall zone for each prime-boost interval onto the prime-boost interval - combined neutralization plane. This projection corresponds to the same scenario illustrated in (a).

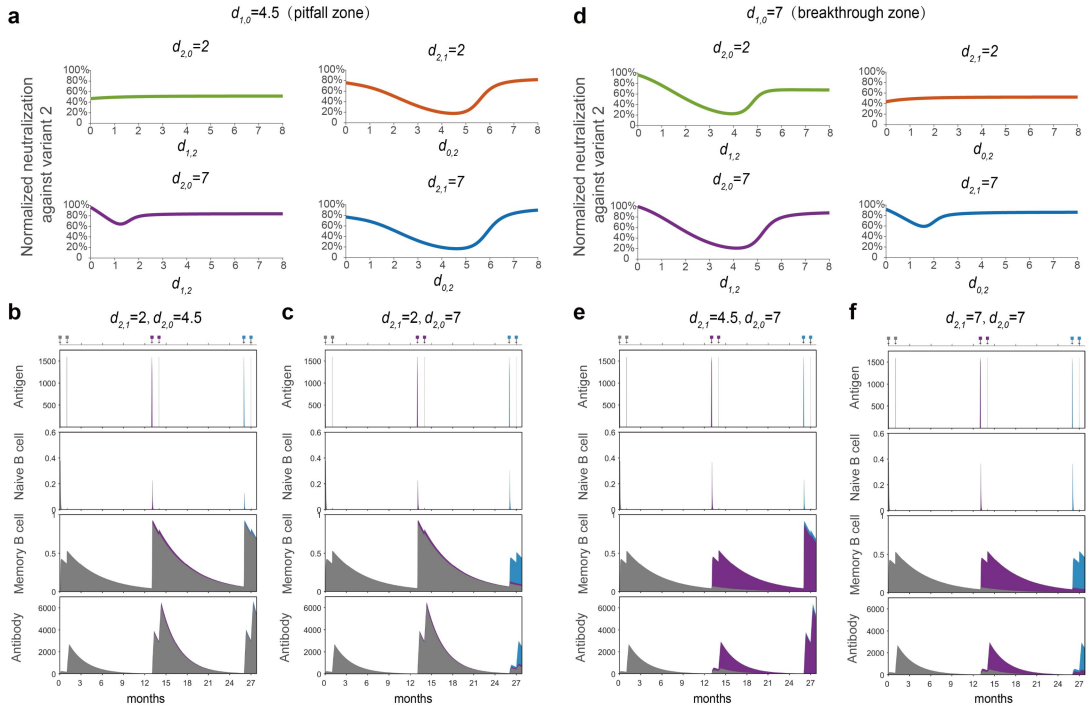

Extended Data Fig. 16 Neutralization profiles and immune dynamics in sequential variant boosting.

a, d, Two-dimensional projections of normalized neutralization against variant 2 (day 824) at different antigenic distances, representing cross-sections of the 3D surfaces in Fig. 6b, c. Panel **a** shows projections when $d_{1,0} = 4.5$ (pitfall zone, Fig. 6b), while panel **d** shows projections when $d_{1,0} = 7$ (breakthrough zone, Fig. 6c). In both panels, the first column displays neutralization profiles at fixed $d_{2,0}$ values (2 and 7) while varying $d_{2,1}$; the second column displays neutralization profiles at fixed $d_{2,1}$ values (2 and 7) while varying $d_{2,0}$.

b, c, e, f, DynaVac simulation of immune dynamics for different combinations of antigenic distances over the extended vaccination sequence. Each panel contains four rows showing: antigen levels (top), naive B cell gross affinity (second row), memory B cell levels (third row), and antibody levels (bottom). Color coding indicates strain specificity: gray (prototype), purple (variant 1), and blue (variant 2). Arrows at the top mark vaccination timepoints. Panel **b** shows dynamics for $d_{1,0} = 4.5$, $d_{2,1} = 2$, $d_{2,0} = 4.5$; panel **c** for $d_{1,0} = 4.5$, $d_{2,1} = 2$, $d_{2,0} = 7$; panel **e** for $d_{1,0} = 7$, $d_{2,1} = 4.5$, $d_{2,0} = 7$; and panel **f** for $d_{1,0} = 7$, $d_{2,1} = 7$, $d_{2,0} = 7$.

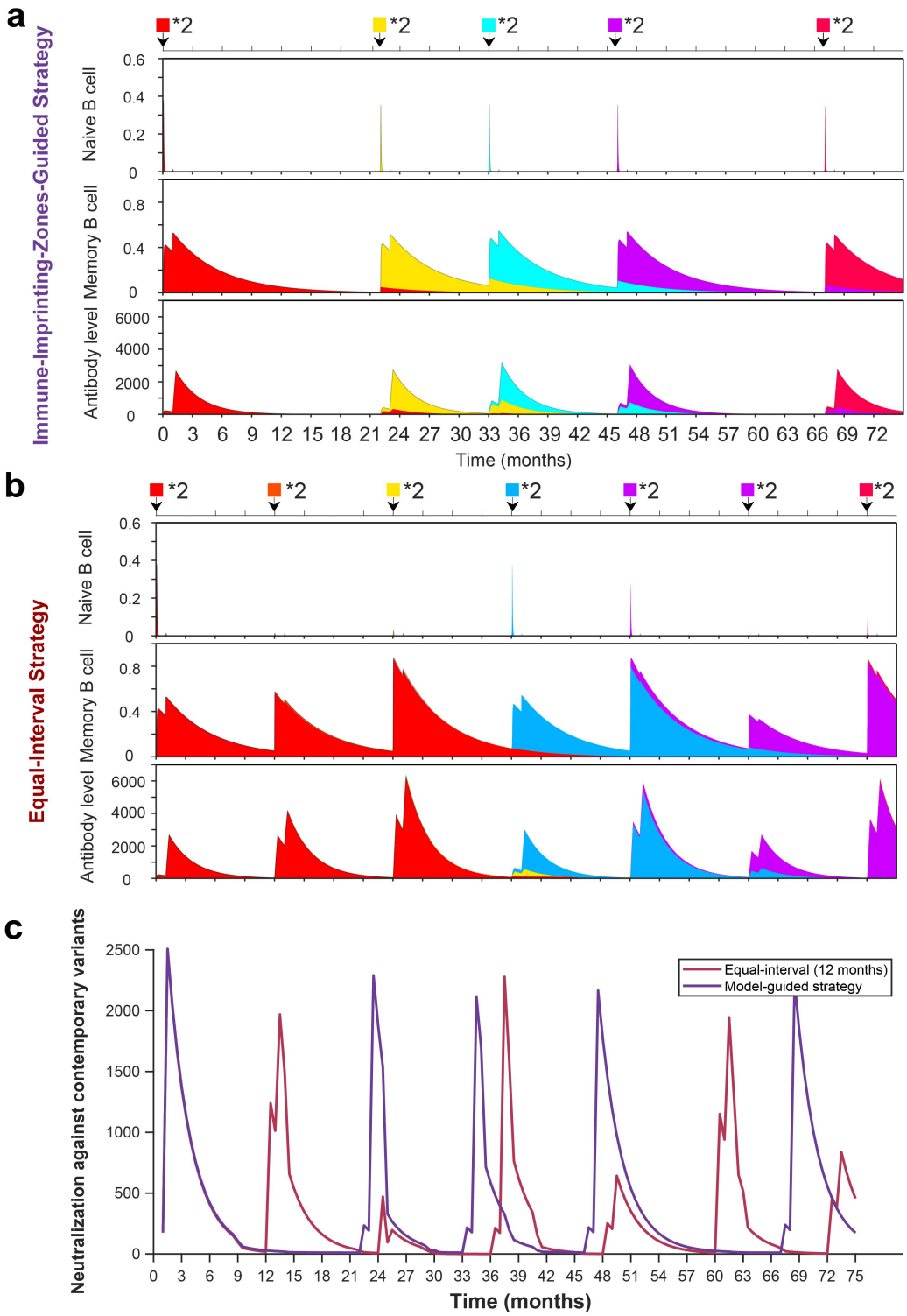

Extended Data Fig. 17 Immune dynamics and neutralization efficacy of model-guided versus empirical vaccination strategies.

a, b, DynaVac simulation of immune dynamics under different vaccination strategies. Time course of key immune components simulated by DynaVac under the model-guided (**a**) and equal-interval (**b**) vaccination strategies shown in Fig. 7c. Top row shows gross affinity of naive B cells, middle row shows memory B cell levels, and bottom row shows antibody levels over time. Colored regions represent variant-specific immune components, with colors matching the corresponding vaccine variants. Arrows marked "×2" at the top of each panel indicate vaccination timepoints with two consecutive boosts administered one month apart.

c, Neutralization against contemporary variants. Time course of neutralization against contemporary circulating variants for model-guided strategy (red line) and equal-interval strategy (purple line). Neutralization was calculated by projecting the variant-specific antibody profiles (shown in bottom panels of **a,b**) onto the dominant circulating variant at each timepoint using cross-neutralization coefficients (Eq.30, Supplementary notes 4). These coefficients were derived from the antigenic distances between variants in the one-dimensional antigenic space, as illustrated in Fig. 7a.

Supplementary Tables

Supplementary Table 1 Original model parameters and estimation of their priori intervals

Symbol	Definition	Units	Priori interval	Reference
P_s	Effective antibody amount per ug spike vaccine	M/ug	[5,30]*10^{-12}	
P_v	Effective antibody amount per ug inactive vaccine	M/ug	[5,30]*10^{-12}	
R_0	mRNA amount per ug mRNA vaccine	M/ug	[0.5,2]*10^{-12}	
k	mRNA translation rate	protein/mRNA/day	[50,500]	24
γ_R	mRNA degradation rate	day^{-1}	[5,10]	25,26
γ_{Ag}	Antigen degradation rate	day^{-1}	[0.001,0.1]	27
γ_{Ab}	Antibody degradation rate	day^{-1}	[0.0001,0.1]	27,28
K	Antigen amount required to occupy half of the maximum load of antigen-presenting cells	M	[1.5, 10]*10^{-9}	29
s_N	Maximum rate of naive B cell affinity maturation	day^{-1}	[5,100]	
p_N	Maximum naive antibody production rate	day^{-1}	[5,400]	
d_N	Naive B cell decay rate	day^{-1}	[0.02,2]	1,21
k_{N2M}	Maximum rate of differentiation of naive B cells into memory B cells	day^{-1}	[0.001,1]	
s_M	Maximum rate of memory B cell proliferation	day^{-1}	[0.05,15]	
p_M	Maximum memory antibody production rate	day^{-1}	[30,1000]	
d_M	memory B cell decay rate	day^{-1}	[0.001,0.01]	1
Ka	Antibody-antigen affinity constant	M^{-1}	[10^8,10^{10}]	30,31
γ_c	Antibody-antigen complex degradation rate	day^{-1}	[10,1000]	30
c_0	Affinity thresholds for cross-reactive differentiation of memory B cells into antibody-secreting plasma cells		[0,0.05]	
m_0	Affinity thresholds for cross-reactive memory B cell proliferation		[0,0.05]	
s_{ini}	Affinity maturation rate during progenitor naive B cells seed the germinal centers	day^{-1}	[0.0005,0.1]	
t_{ini}	Interval between vaccination and onset of antibody production	day	[0.5,2]	1,21
t_{min}	Minimum humoral immune response duration	day	[5,20]	1,21,32
t_{max}	Maximum humoral immune response duration	day	[20,60]	1,21,32

Supplementary Table 2 Reduced model parameters and estimates after parameterized on different datasets

Symbol	Definition	Units	Priori interval	Trained by dataset from this study (mice)	Trained by Yisimayi, et.al. dataset (mice)	Trained by combined dataset (mice)	Trained by clinical trial (human)
P_s[b]	Effective antigen amount per ug spike vaccine	10^{-12}M/ug	[5,30]		7.436	14.52	
P_v	Effective antigen amount per ug inactive vaccine (CoronaVac)	10^{-12}M/ug	[5,30]	9.203	5.671	7.395	22.75
P_r[a]	Equivalent antigen amount per ug mRNA vaccine in this study	10^{-12}M/ug	[50,300]	75.21		150.0	52.94
$P_r^{'}$[b]	Equivalent antigen amount per ug mRNA vaccine in Yisimayi, et.al. dataset	10^{-12}M/ug	[50,300]		290.1	277.4	
γ_{Ag}	Antigen degradation rate	day^{-1}	[0.001,0.1]	0.01152	0.01404	0.01939	0.03543
γ_{Ab}	Antibody degradation rate	day^{-1}	[0.0001,0.1]	0.001033	0.0004281	0.0007187	0.013417
K	Antigen amount required to occupy half of the maximum load of antigen-presenting cells	10^{-12}M	[100,1000]	525.6	750.8	527.7	547.1
s_N	Maximum rate of naive B cell affinity maturation	day^{-1}	[5,100]	32.88	67.90	38.93	6.351
p_N	Maximum naive antibody production rate	day^{-1}	[100,500]	211.2	177.5	154.3	352.9
d_N	Naive B cell decay rate	day^{-1}	[0.02,2]	2.071	2.462	1.724	0.8879
k_{N2M}	Maximum rate of differentiation of naive B cells into memory B cells	day^{-1}	[0.001,1]	0.0793	0.1491	0.1116	0.8188
s_M	Maximum rate of memory B cell proliferation	day^{-1}	[1,20]	15.93	6.869	11.92	7.148
p_M	Maximum memory antibody production rate	day^{-1}	[100,2000]	1646	1076	1167	540.5
d_M	memory B cell decay rate	day^{-1}	[0.001,0.01]	0.002611	0.001428	0.001762	0.007101
γ_{neu}^{Delta}[a]	Delta specific Antibody-antigen neutralization rate	$10^{12}M^{-1}day^{-1}$	[0.001,1]	0.05503		0.05144	0.07493
γ_{neu}^{BA5}[b]	BA.5 specific Antibody-antigen neutralization rate	$10^{12}M^{-1}day^{-1}$	[0.001,1]		0.03370	0.05144	

Symbol	Definition	Units	Priori interval	Trained by dataset from this study	Trained by Yisimayi, et.al. dataset	Trained by combined dataset	Trained by human clinical trial
c_0	Affinity threshold for cross-reactive differentiation of memory B cells into antibody-secreting plasma cells		[0,0.05]	$1.353*10^{-5}$	$1.553*10^{-5}$	$1.046*10^{-5}$	$3.421*10^{-5}$
m_0	Affinity threshold for cross-reactive memory B cell proliferation		[0,0.05]	$6.422*10^{-4}$	$5.285*10^{-4}$	$8.451*10^{-4}$	$7.144*10^{-3}$
s_{ini}	Affinity maturation rate during progenitor naive B cells seed the germinal centers	day^{-1}	[0.0005,0.1]	0.08157	0.06778	0.05527	0.01924
t_{ini}	Interval between vaccination and onset of antibody production	day	[0.5,2]	0.7955	1.001	1.05	1.062
t_{min}	Minimum humoral immune response duration	day	[5,20]	14.02	13.42	16.10	9.769
t_{max}	Maximum humoral immune response duration	day	[20,60]	51.64	46.04	35.97	21.15
$C_{7,1}$[a]	Corrected titer of CoronaVac against BA.5		[0,15]	11.93		11.93	11.93
$C_{8,1}$[a]	Corrected titer of CoronaVac against BF.7		[0,15]	14.49		14.49	14.49
$C_{9,1}$[a]	Corrected titer of CoronaVac against BQ.1.1		[0,15]	14.68		14.68	14.68
$C_{10,1}$[a]	Corrected titer of CoronaVac against XBB.1.5		[0,15]	15.00		15.00	15.00
$C_{11,1}$[a]	Corrected titer of CoronaVac against JN.1		[0,15]	1.585		1.585	1.585
$C_{10,2}$[a]	Corrected titer of Alpha/beta against XBB.1.5		[0,15]	5.631		5.631	5.631
$C_{10,3}$[a]	Corrected titer of Delta against XBB.1.5		[0,15]	2.963		2.963	2.963
$C_{10,4}$[a]	Corrected titer of BA.1 against XBB.1.5		[0,15]	0.2758		0.2758	0.2758
$f_{CoronaVac}^{Delta}$[a]	Relative self-neutralization ratio between Prototype and Delta in this study		[0.1,2]	0.1962		0.2816	0.3235
$f_{CoronaVac}^{BA5}$[b]	Relative self-neutralization ratio between wild type inactive vaccine and Delta spike vaccine in Yisimayi, et.al. dataset.		[0.1,2]		0.6526	0.9976	
f_{mRNA}^{BA5}[b]	Relative self-neutralization ratio between wild type mRNA vaccine and Delta spike vaccine in Yisimayi, et.al. dataset.		[0.1,2]		0.1073	0.2131	

[a] Parameters exclusive to the dataset from this study
[b] Parameters exclusive to the Yisimayi, et al. dataset

Supplementary Table 3 Raw pseudovirus titers for homologous vaccinations regimens

		Vaccine (antibody)						
		CoronaVac	alpha/beta	delta	BA.1	BA.2/5	XBB.1.5	JN.1
Pseudovirus (antigen)	Prototype	1713.0	260.3	1620.3	58.6	145.6	912.9	910.2
	alpha	1102.0	1780.1	1953.1	71.9	87.6	771.2	558.3
	beta	570.0	1163.8	1545.8	140	187.7	300.5	274.5
	delta	94.3	141.3	6210.7	107.2	358.8	136.6	23.6
	BA.1	33.6	115.5	281.5	1807.8	527.9	34.5	242.3
	BA.2	18.6	58.2	212.4	185.9	2598.4	2795.7	1028.7
	BA.5	$C_{7,1}(15.0)$	23.4	153	67.7	1775.9	6848.5	1811.7
	XBB.1.5	$C_{10,1}(15.0)$	$C_{10,2}(15.0)$	$C_{10,3}(17.6)$	$C_{10,4}(17.4)$	209.6	33068.8	298.1
	JN.1	$C_{11,1}(15.0)$	19.5	86.6	23.4	25.8	370.5	29148.9

Note: Due to technical limitations, the lowest measurable titer is 15. For those data with a titer close to 15, the titers are set as unknown parameters greater than 0 and less than 15.

Supplementary Table 4 Antigen-antibody titer matrix

		Antibody						
		CoronaVac	alpha/beta	delta	BA.1	BA.2/5	XBB.1.5	JN.1
Antigen	Prototype	1713.0	260.3	1620.3	58.6	145.6	912.9	910.2
	alpha/beta	792.6	1439.3	1737.6	100.3	128.2	481.4	391.5
	delta	94.3	141.3	6210.7	107.2	358.8	136.6	23.6
	BA.1	33.6	115.5	281.5	1807.8	527.9	34.5	242.4
	BA.2/5	$\sqrt{18.6 * C_{7,1}}$	23.4	153	67.7	1775.9	6848.5	1365.2
	XBB.1.5	$C_{10,1}$	$C_{10,2}$	$C_{10,3}$	$C_{10,4}$	209.6	33068.8	298.1
	JN.1	$C_{11,1}(15.0)$	19.5	86.6	23.4	25.8	370.5	29148.9

Supplementary Table 5 Self-neutralization titers and relative self-neutralization ratio

Antigen	CoronaVac	alpha/beta	delta	BA.1	BA.2/5	XBB.1.5	JN.1
Self-neutralization titers	1713.0	1439.3	6210.7	1807.8	2148.1	33068.8	29148.9
relative self-neutralization ratio	$f^{\text{Delta}}_{CoronaVac}$	0.231	1	0.291	0.346	5.32	4.70

Supplementary Table 6 Cross-neutralization matrix

		Antibody						
		CoronaVac	alpha/ beta	delta	BA.1	BA.2/5	XBB.1.5	JN.1
Antigen	Prototype	1.0000	0.1808	0.2609	0.0324	0.0678	0.0112	0.0312
	alpha/beta	0.4627	1.0000	0.2798	0.0555	0.0597	0.0146	0.0134
	delta	0.0551	0.0982	1.0000	0.0593	0.1670	0.0041	0.0008
	BA.1	0.0196	0.0802	0.0453	1.0000	0.2457	0.0010	0.0083
	BA.2/5	$\frac{\sqrt{18.6 * C_{7,1}}}{1713}$	0.0256	0.0290	0.0621	1.0000	0.1323	0.0468
	XBB.1.5	$\frac{C_{10,1}}{1713}$	$\frac{C_{10,2}}{1440}$	$\frac{C_{10,3}}{6211}$	$\frac{C_{10,4}}{1808}$	0.0084	1.0000	0.0102
	JN.1	$\frac{C_{11,1}}{1713}$	0.0135	0.0139	0.0129	0.0120	0.0112	1.0000

Supplementary Table 7 Raw titration data from the homologous vaccination regimens against the 11 pseudoviruses

		Vaccine (antibody)						
		CoronaVac	alpha/beta	delta	BA.1	BA.2/5	XBB.1.5	JN.1
Pseudovirus	Prototype	1713.0	260.3	1620.3	58.6	145.6	912.9	910.2
	alpha	1102.0	1780.1	1953.1	71.9	87.6	771.2	558.3
	beta	570.0	1163.8	1545.8	140	187.7	300.5	274.5
	delta	94.3	141.3	6210.7	107.2	358.8	136.6	23.6
	BA.1	33.6	115.5	281.5	1807.8	527.9	34.5	242.4
	BA.2	18.6	58.2	212.4	185.9	2598.4	2795.7	1028.7
	BA.5	$C_{7,1}(15.0)$	23.4	153	67.7	1775.9	6848.5	1811.7
	BF.7	$C_{8,1}(15.0)$	26.2	98.7	34.5	1801.6	4685.9	2854.6
	BQ.1.1	$C_{9,1}(15.0)$	32.7	29.0	30.9	329.9	662.1	667.6
	XBB.1.5	$C_{10,1}(15.0)$	$C_{10,2}(15.0)$	$C_{10,3}(17.6)$	$C_{10,4}(17.4)$	209.6	33068.8	298.1
	JN.1	$C_{11,1}(15.0)$	19.5	86.6	23.4	25.8	370.5	29148.9

Note: Due to detection limitations, titers around the detection limit (15) were considered as unknown parameters bounded between 0 and 15.

Supplementary Table 8 Antibody-pseudovirus cross-neutralization matrix

		Vaccine (antibody)						
		CoronaVac	alpha/beta	delta	BA.1	BA.2/5	XBB.1.5	JN.1
Pseudovirus	Prototype	1.0000	0.1808	0.2609	0.0324	0.0678	0.0276	0.0312
	alpha	0.6433	1.2368	0.3145	0.0398	0.0408	0.0233	0.0192
	beta	0.3328	0.8086	0.2489	0.0774	0.0874	0.0091	0.0094
	delta	0.0551	0.0982	1.0000	0.0593	0.1670	0.0041	0.0008
	BA.1	0.0196	0.0802	0.0453	1.0000	0.2457	0.0010	0.0083
	BA.2	0.0108	0.0404	0.0342	0.1028	1.2096	0.0845	0.0353
	BA.5	$C_{7,1}$/1713	0.0163	0.0246	0.0374	0.8267	0.2071	0.0622
	BF.7	$C_{8,1}$/1713	0.0182	0.0159	0.0191	0.8387	0.1417	0.0979
	BQ.1.1	$C_{9,1}$/1713	0.0227	0.0047	0.0171	0.1536	0.0200	0.0229
	XBB.1.5	$C_{10,1}$/1713	$C_{10,2}$/1440	$C_{10,3}$/6211	$C_{10,4}$/1808	0.0976	1.0000	0.0102
	JN.1	$C_{11,1}$/1713	0.0135	0.0139	0.0129	0.0120	0.0112	1.0000

Note: Due to detection limitations, titers around the detection limit (15) were considered as unknown parameters bounded between 0 and 15.

Supplementary Table 9 Raw pseudovirus titer data for homologous vaccination regimens in Yisimayi, et.al. dataset

		Vaccines (antibody)				
		Prototype (CoronaVac)	Prototype (mRNA)	BA.5 (spike)	BQ.1.1 (spike)	XBB.1.5 (spike)
pseudovirus (antigen)	Prototype	3236	27330	43	31	31
	BA.5	97	648	21949	5213	383
	BQ.1.1	31	257	4100	14357	795
	XBB.1.5	30	83	73	139	5561

Supplementary Table 10 Self-neutralization titers and relative self-neutralization ratios in Yisimayi, et.al. dataset

Antigen	Prototype (CoronaVac)	Prototype (mRNA)	BA.5 (spike)	BQ.1.1 (spike)	XBB.1.5 (spike)
Self-neutralization titers	3236	27330	21949	14357	5561
relative self-neutralization ratio	$f^{BA5}_{CoronaVac}$	f^{BA5}_{mRNA}	1.0000	0.6541	0.2534

Supplementary Table 11 Cross-neutralization matrix in Yisimayi, et.al. dataset

		Vaccines (antibody)				
		Prototype (CoronaVac)	Prototype (mRNA)	BA.5 (spike)	BQ.1.1 (spike)	XBB.1.5 (spike)
pseudovirus (antigen)	Prototype	1.0000	1.0000	0.0020	0.0022	0.0056
	BA.5	0.0300	0.0237	1.0000	0.3631	0.0689
	BQ.1.1	0.0096	0.0094	0.1868	1.0000	0.1430
	XBB.1.5	0.0030[a]	0.0030	0.0033	0.0097	1.0000

[a] Due to technical limitations, the neutralization titer of CoronaVac against XBB.1.5 reached the lower detection limit. Therefore, when calculating the cross-neutralization coefficient of CoronaVac against XBB.1.5, the cross-neutralization coefficient of the prototype mRNA vaccine against XBB.1.5 was used as a substitute.

Supplementary Table 12 The mutation sites of the SARS-Cov-2 variant mRNA vaccines campare to propotype Spike protein

Vaccine	Company	Information	Cat#	Mutation sites	Number of mutations
CoronaVac	Sinovac BIotech	Prototype		-	/
RQ3013	Walvax Biotechnology Co	Alpha/Beta	RQ3013	DelH69-V70、DelY144、K417N、E484K、N501Y、A570D、D614G、P681H、R682G、R683S、R685S、A701V、T716I、S982A、D1118H	16
RQ3014	Walvax Biotechnology Co	Delta	RQ3014	T19R、G142D、DelF157-R158、L452R、T478K、D614G、P681R、R682G、R683S、R685S、D950N、K986P、V987P	14
RQ3021	Walvax Biotechnology Co	Omicron BA.1	RQ3021	A67V、DelH69-V70、T95I、G142D、DelVYY143/145、N211I、DelL212、ins214EPE、G339D、S371L、S373P、S375F、K417N、N440K、G446S、S477N、T478K、E484A、Q493R、G496S、Q498R、N501Y、Y505H、T547K、D614G、H655Y、N679K、P681H、R682G、R683S、R685S、N764K、D796Y、N856K、Q954H、N969K、L981F、K986P、V987P	44
RQ3019	Walvax Biotechnology Co	Omicron BA.2/4/5	RQ3019	T19I、LPPA24S、G142D、V213G、G339D、S371F、S373P、S375F、T376A、D405N、R408S、K417N、N440K、L452R、S477N、T478K、E484A、F486V、Q493R、Q498R、N501Y、Y505H、D614G、H655Y、N679K、P681H、R682G、R683S、R685S、N764K、D796Y、Q954H、N969K	36
RQ3033	Walvax Biotechnology Co	XBB.1.5	RQ3033	T19I、LPPA24S、V83A、G142D、DelY144、H146Q、Q183E、V213E、G252V、G339H、R346T、L368I、S371F、S373P、S375F、T376A、D405N、R408S、K417N、N440K、V445P、G446S、N460K、S477N、T478K、E484A、F486P、F490S、Q498R、N501Y、Y505H、D614G、H655Y、N679K、P681H、R682G、R683S、R685S、N764K、D796Y、Q954H、N969K	45
RQ3064	Walvax Biotechnology Co	JN.1	RQ3064	T19I、L21R, LPPA24S、S50L、DelH69、DelV70、V127F、G124D、DelY144、DelN211、L212I、V213G、L216F、H245N、A264D、G339H、K356T、S371F、S373P、S375F、T376A、R403K， D405N、R408S、K417N、N440K、V445H、G446S、N450D、L452W、L455S、N460K、S477N、T478K、N481K、DelV483、E484K、F486P、Q498R、N501Y、Y505H、E554K、A570V、D614G、P621S、H655Y、P681R、P682G、R683S、R685S、N764K、D796Y、S939F、Q954H、N969K	58
RQ3025	Walvax Biotechnology Co	Alpha/Beta+Omicron BA.2/4/5	RQ3025	T19I、LPPA24S、DelH69、DelV70、G142D、DelY144、V213G、G339D、S371F、S373P、S375F、T376A、D405N、R408S、K417N、N440K、L452R、S477N、T478K、E484K、E484A、F486V、Q493R、Q498R、N501Y、Y505H、A570D、D614G、H655Y、N679K、P681H、R682G、R683S、R685S、A701V、T716I、N764K、D796Y、Q954H、N969K、S982A、D1118H	45
RQ3027	Walvax Biotechnology Co	Alpha/Beta+XBB.1.5	RQ3027	T19I、LPPA24S、DelH69-V70、V83A、G142D、DelY144、H146Q、Q183E、V213E、G252V、G339H、R346T、L368I、S371F、S373P、S375F、T376A、D405N、R408S、K417N、N440K、V445P、G446S、N460K、S477N、T478K、E484A、E484K、F486P、F490S、Q498R、N501Y、Y505H、A570D、D614G、H655Y、N679K、P681H、R682G、R683S、R685S、A701V、T716I、N764K、D796Y、Q954H、N969K、S982A、D1118H	53

Supplementary Table 13 The mutantions of SARS-CoV-2 pseudovirus on Spike protein

SARS-CoV-2 sublineages	Mutations	Number of mutations
Prototype	/	/
Alpha (B.1.1.7)	DEL69/70, DEL144/144, N501Y, A570D, D614G, P681H, T716I, S982A, D1118H	10
Beta (B.1.351)	D80A, D215G, DEL241/243, K417N, E484K, N501Y, D614G, A701V	10
Delta (B.1.617.2)	T19R, E156G, DEL157/158, L452R, T478K, D614G, P681R, D950N	9
BA.1	A67V, DEL69-70, T95I, G142D, DEL143-145, N211I, DEL212/212, INS214EPE, G339D, S371L, S373P, S375F, K417N, S477N, T478K, E484A, Q493R, G496S, Q498R, N501Y, Y505H, T547K, D614G, H655Y, N679K,P681H, N764K, D796Y, N856K, Q954H, N969K, L981F	37
BA.2	T19I, L24S, DEL25-27, G142D, V213G, G339D, S371F, S373P, S375F, T376A, D405N, R408S, K417N, N440K, S477N, T478K, E484A, Q493R, Q498R, N501Y, Y505H, D614G, H655Y, N679K, P681H, N764K, D796Y, Q954H, N969K	31
BA.4/5	T19I, L24S, DEL25-27, DEL69-70, G142D, V213G, G339D, S371F, S373P, S375F, T376A, D405N, R408S, K417N, N440K, L452R, S477N, T478K, E484A, F486V, Q498R, N501Y, Y505H, D614G, H655Y, N679K, P681H, N764K, D796Y, Q954H, N969K	34
BF.7	T19I, L24S, DEL25-27, DEL69-70, G142D, V213G, G339D, R346T, S371F, S373P, S375F, T376A, D405N, R408S, K417N, N440K, L452R, S477N, T478K, E484A, F486V, Q498R, N501Y, Y505H, D614G, H655Y, N679K, P681H, N764K, D796Y, Q954H, N969K	35
BQ.1.1	T19I, L24S, DEL25-27, DEL69-70, G142D, V213G, G339D, R346T, S371F, S373P, S375F, T376A, D405N, R408S, K417N, N440K, K444T, L452R, N460K, S477N, T478K, E484A, F486V, Q498R, N501Y, Y505H, D614G, H655Y, N679K, P681H, N764K, D796Y, Q954H, N969K	37
XBB.1.5	T19I, L24S, DEL25-27, V83A, G142D, DEL144 H146Q, Q183E, V213E, G252V, G339H, R346T, L368I, S371F, S373P, S375F, T376A, D405N, R408S, K417N, N440K, V445P, G446S, N460K, S477N, T478K, E484A, F486P, F490S, Q498R, N501Y, Y505H, D614G, H655Y, N679K, P681H, N764K, D796Y, Q954H, N969K	42
JN.1	T19I, L24S, DEL25-27, S50L, DEL69-70, V127F, G142D, DEL144, F153S, R158G, N211I, DEL212, V213G, L216F, H245N, A264D, I332V, G339H, K356T, S371F, S373P, S375F, T376A, R403K, D405N, R408S, K417N, N440K, V445H, G446S, N450D, L452W, L455S, N460K, S477N, T478K, N481K, E484K, F486P, Q498R, N501Y, Y505H, E554K, A570V, D614G, P621S, H655Y, N679K, P681R, N764K, D796Y, S939F, Q954H, N969K, P1143L	58

Supplementary Tables 14 to 18 are provided as an Excel file, available in the supplementary materials.